UNIVERSIDAD DE INVESTIGACIÓN DE TECNOLOGÍA EXPERIMENTAL YACHAY

Escuela de Ciencias Químicas e Ingeniería

Exploring polymer-ionic solution interactions: An In-Depth study chitosan-starch matrix in near neutral electrolytes for zinc-air batteries

Trabajo de titulación presentado como requisito para la obtención del título de Magister en Ciencias Químicas con Mención en Materiales

Author:

Vaca Chacón Sara Lizeth

Tutor:

Tafur Juan Pablo, PhD

Co-Tutor:

Morera Córdova Vivian, PhD

Urcuquí, julio 2024

AUTORÍA

Yo, **SARA LIZETH VACA CHACÓN**, con cédula de identidad 1004036065, declaro que las ideas, juicios, valoraciones, interpretaciones, consultas bibliográficas, definiciones y conceptualizaciones expuestas en el presente trabajo; así cómo, los procedimientos y herramientas utilizadas en la investigación, son de absoluta responsabilidad de la autora del trabajo de titulación.

Así mismo, me acojo a la normativa interna de la Universidad de Investigación de Tecnología Experimental Yachay.

San Miguel de Urcuquí, Julio 2024

_____

Sara Vaca

CI: 1004036065

AUTORIZACIÓN DE PUBLICACIÓN

Yo, **SARA LIZETH VACA CHACÓN**, con cédula de identidad 1004036065, cedo a la Universidad de Investigación de Tecnología Experimental Yachay, los derechos de publicación de la presente obra, sin que deba haber un reconocimiento económico por este concepto. Declaro además que el texto del presente trabajo de titulación no podrá ser cedido a ninguna empresa editorial para su publicación u otros fines, sin contar previamente con la autorización escrita de la Universidad.

Asimismo, autorizo a la Universidad que realice la digitalización y publicación de este trabajo de integración curricular en el repositorio virtual, de conformidad a lo dispuesto en el Art. 144 de la Ley Orgánica de Educación Superior.

San Miguel de Urcuquí, Julio 2024

_____

Sara Vaca

CI: 1004036065

Dedication

To my lovely husband who has always been my support and has pushed me to be a better person every day. I dedicate this merit to him.

To my wonderful family, including my mother-in-law and father-in-law, who have always been there for me and treated me like their own daughter. Your love and support have been invaluable throughout this journey

Sara Vaca

Acknowledgments

<div align="right">Sara Vaca</div>

Table of Contents

List of Figures

List of Tables

Resumen

Ante el aumento de la demanda mundial de energía y la búsqueda crítica de soluciones energéticas sostenibles, esta investigación profundiza en el comportamiento electrolítico de hidrogeles biopoliméricos derivados de quitosano y almidón en soluciones iónicas casi neutras dentro de un sistema $ZnCl_2$ + NH_4Cl, modulado a través de diferentes niveles de pH para mejorar el rendimiento de las baterías de zinc-aire (ZABs). El estudio evalúa el impacto del pH de la solución iónica sobre las propiedades estructurales, morfológicas, térmicas, y electroquímicas de los hidrogeles en prototipos primarios de ZABs. Notablemente, a un pH casi neutro de 7.00, el electrolito de gel polimérico demostró una conductividad iónica superior (0.11 $S.cm^{-1}$) y una capacidad específica (675 $mAh.g^{-1}$), revelando menores resistencias de volumen y mayores capacidades específicas. El análisis térmico reveló una mejor estabilidad de los sistemas de gel polimérico a valores de pH de 6.00 y 7.00, los ensayos de Microscopía Electrónica de Barrido (SEM) mostraron microestructuras uniformes y cohesivas atribuidas a la formación estable de complejos zinc-amina. La Espectroscopía Infrarroja por Transformada de Fourier (FTIR) resaltó variaciones dependientes del pH en las bandas vibracionales de los grupos funcionales, influyendo en las interacciones de iones de zinc y en el rendimiento electroquímico. El análisis por Difracción de Rayos X (XRD) subrayó la ausencia de productos precipitados sólidos a pH 7.00, mejorando así la movilidad iónica y la conductividad. En consecuencia, los hallazgos sugieren que mantener condiciones de pH casi neutro aumenta sustancialmente las propiedades físicas y electroquímicas de las ZABs, presentando una vía prometedora para soluciones de almacenamiento de energía sostenibles.

Palabras clave: baterías de zinc-aire, electrolito casi neutro, hidrogeles

Abstract

In light of the escalating global energy demands and the critical pursuit of sustainable energy solutions, this research delves into the electrolytic behavior of biopolymeric hydrogels derived from chitosan and starch in near-neutral ionic solutions within a $ZnCl_2$ + NH_4Cl system, modulated across varying pH levels to enhance zinc-air battery (ZAB) performance. The study evaluates the impact of ionic solution pH on the structural, morphological, thermal, and electrochemical properties of the hydrogels in primary ZAB prototypes. Remarkably, at a near-neutral pH value of 7.00, the polymer gel electrolyte demonstrated superior ionic conductivity (0.11 $S.cm^{-1}$), and specific capacity (675 $mAh.g^{-1}$), revealing lower volume resistances and higher specific capacitances. Thermal analysis revealed enhanced stability of the polymer gel systems at elevated pH levels, corroborated by Scanning Electron Microscopy (SEM) which confirmed uniform, cohesive microstructures attributed to stable zinc-amine complex formation. Fourier Transform Infrared Spectroscopy (FTIR) indicated pH-dependent variations in the vibrational bands of functional groups, influencing zinc ion interactions and electrochemical performance. X-ray Diffraction (XRD) analysis underscored the absence of solid precipitate products at pH value of 7.00, thereby improving ionic mobility and conductivity. Consequently, the findings suggest that maintaining near-neutral pH conditions substantially increase the physical and electrochemical properties of ZAB, presenting a promising avenue for sustainable energy storage solutions.

Keywords: zinc-air batteries, near-neutral electrolyte, hydrogels

Chapter 1: Introduction

1.1. Overview of Electrochemical Energy Storage

Electrochemical energy storage is a highly efficient solution to mitigate the escalating energy and environmental challenges. In this sense, electrochemical energy storage systems (EES) play an important role in offering solutions for a range of applications from portable electronics to large-scale grid storage [1]. These systems store energy in chemical form and convert it back to electrical energy when needed [2]. The basic principle consists of redox reactions taking place at the electrodes within an electrolytic medium. The three primary types of electrochemical energy storage systems are batteries, supercapacitors, and fuel cells [3].

1.2. Zinc-Air Batteries (ZABs)

ZABs are a type of battery that generates electricity through the oxidation of zinc by oxygen from the air, offering advantages such as low cost, high safety, and environmental friendliness [4]. In ZABs, the primary components that play crucial roles in the system's functionality are the zinc anode, air cathode, and electrolyte, play crucial roles in the functionality of ZABs.

Zinc anode: In ZABs, the zinc anode is a vital source of energy. It goes through oxidation during discharging. Hence, the zinc forms zinc oxide, releasing electrons moving along the outer circuit and producing electricity [5].

Air cathode: mainly made up of porous structures through which the air diffuses into the electrode giving room for a large surface area in which oxygen reduction reaction (ORR) occurs. Carbon-based materials with manganese dioxide (MnO_2) as catalyst and Platinum are commonly used as air cathodes because this material improves ORR [6].

Electrolyte: they can be either liquid or gel. Aqueous electrolytes, often based on potassium hydroxide (KOH), are commonly used due to their high ionic conductivity and ability to promote electrochemical reactions. On the other hand, gel electrolytes, incorporating polymers such as polyvinyl alcohol (PVA) or polyacrylic acid (PAA), offer

the advantage of reduced leakage and improved mechanical stability, making them suitable for flexible and wearable applications [7].

The high energy density of ZABs, combined with their low cost and environmental benefits, makes them suitable for a wide range of applications. They are commonly used in hearing aids, remote sensors, and other portable electronic devices. However, their widespread adoption is hindered by challenges like limited life cycle and slow kinetics, particularly in the oxygen reduction and evolution reactions [8]. Efforts to overcome these problems include developing advanced catalysts and electrode materials to enhance reaction kinetics and strategies to prevent zinc dendrite formation and corrosion [9], [10]. Research into hybrid electrolyte systems aims to improve ionic conductivity and mechanical stability, addressing leakage and volatility concerns [11] ,[12], [13]. These advancements are crucial for maximizing the potential of ZABs in applications like portable electronics, electric vehicles, and grid energy storage.

1.2.1. Primary Zinc-Air Batteries

This type of battery cannot be recharged once the chemical reactants are consumed. Primary ZABs, commercialized since 1930s, are known for their high energy density, safety, and low cost, making them suitable for hearing aids and navigation lights [14]. They feature a zinc anode with an alkaline electrolyte and a carbon cathode with a MnO_2 catalyst. Their discharge mechanism involves oxygen reduction reaction (ORR) (Equation 3) and zinc oxidation (Equation 1) in an alkaline medium [15]:

Anode: $Zn + 4(OH)^- \rightarrow Zn(OH)_4^{2-} + 2e^-$, $E^0 = -1.25V \; vs. SHE$ **Eq.1**

Complexation: $Zn(OH)_4^{2-} \rightarrow ZnO + H_2O + 2OH^-$ **Eq.2**

Cathode: $0.5O_2 + H_2O + 2e^- \rightarrow 2OH^- \;\; E^0 = 0.40V \; vs. SHE$ **Eq.3**

Overall reaction: $0.5O_2 + Zn \leftrightarrow ZnO \;\;\; E^0 = 1.65V \; vs. SHE$ **Eq.4**
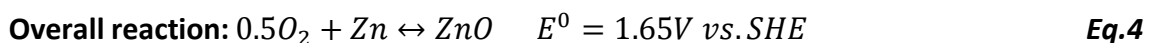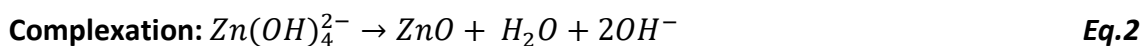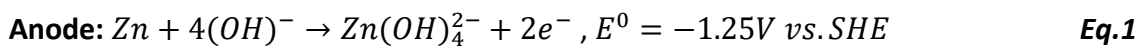
Moreover, commercial primary ZABs offer up to 1400 Wh. L^{-1} and can operate within a wide temperature range from -10 to 55 °C. Additionally, these batteries can be stored for extended periods without losing their discharge capacity, provided that the air intake is properly protected [16].

1.2.1. Secondary Zinc Air Batteries

Secondary or rechargeable ZABs are characterized by their ability to provide energy repeatedly due to the regeneration of the active materials that make up the cell. In ZABs with an alkaline aqueous electrolyte, zinc oxidizes during discharge, forming ZnO. For the system to be rechargeable, the zinc anode must be regenerated. This regeneration can be achieved through mechanical, hydraulic, or electrical recharging methods [17].

This system relies on the electrical recharge of active materials; specifically, ZnO formed during discharge is reduced during charging to reform metallic zinc (Equation 8). Similarly, reduced oxygen undergoes oxidation during charging (Equation 11), producing oxygen in the oxygen evolution reaction (OER). In traditional electrically rechargeable zinc-air systems, an alkaline aqueous electrolyte is used, and the reactions during discharge and charge are as follows [17]:

Discharge

Zinc electrode: $Zn + 4(OH)^- \rightarrow Zn(OH)_4^{2-} + 2e^-$ **Eq.5**

$Zn(OH)_4^{2-} \rightarrow ZnO + H_2O + 2OH^-$ **Eq.6**

Air electrode: $\frac{1}{2}O_2 + H_2O + 2e^- \rightarrow 2OH^-$ **Eq.7**

Overall reaction: $Zn + \frac{1}{2}O_2 \rightarrow ZnO$ **Eq.8**

Charge

Zinc electrode: $ZnO + H_2O + 2OH^- \rightarrow Zn(OH)_4^{2-}$ **Eq.9**

$Zn(OH)_4^{2-} + 2e^- \rightarrow Zn + 4OH^-$ **Eq.10**

Air electrode: $2OH^- \rightarrow \frac{1}{2}O_2 + H_2O + 2e^-$ **Eq.11**

Overall reaction: $ZnO \rightarrow Zn + \frac{1}{2}O_2$ **Eq.12**
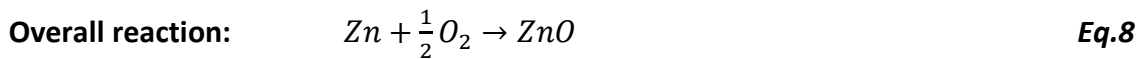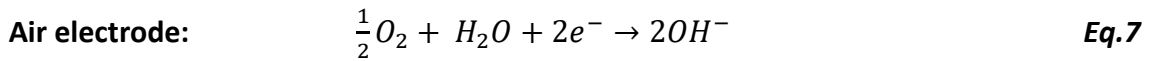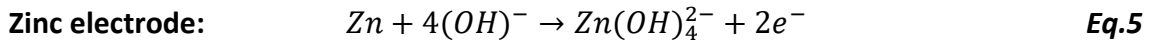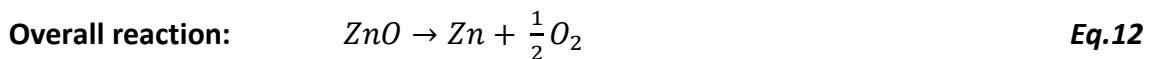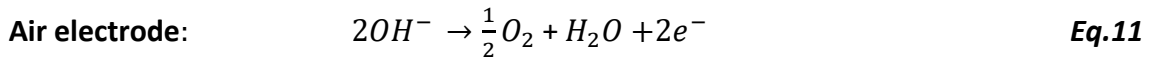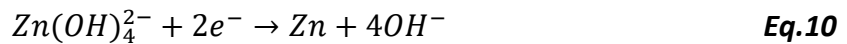
Nevertheless, The ORR and OER at the air electrode are slow due to the complex multi-electron transfer processes involved. This results in high polarization; therefore, a significant voltage difference is required to drive these reactions, which reduces the battery's efficiency and reversibility [18].

1.2.3. Theoretical Specific Energy, Energy Density and Specific Capacity

ZABs are notable for their high theoretical specific energy, energy density, and specific capacity. The theoretical specific energy of ZABs is approximately 1 218 $Wh.kg^{-1}$, making them ideal for applications requiring lightweight energy storage, such as portable electronics and electric vehicles [19], [20], [21]. Their theoretical energy density is about 6 136 $Wh. L^{-1}$, which is crucial for space-constrained applications, allowing significant energy storage in a small volume [22].

The specific capacity of ZABs is around 820 $mAh.g^{-1}$, reflecting the efficient use of zinc as the anode material [23], [24]. These data indicate that ZABs can provide substantial energy and power while remaining cost-effective and environmentally friendly.

1.2.4. Challenges in rechargeable ZABs

ZABs have high energy density, but their use is limited by several major challenges that affect their performance and practicality, especially in industrial applications that require fast discharge and recharge [25]. The main issues include shorter life cycles, slower reaction speeds, and the formation of dendrites.

Shorter Life Cycle: One of the challenges of ZABs is their shorter cycle life compared to other battery technologies. The repetitive cycling causes degradation of the zinc anode due to their exposure to air which introduces complications such as CO_2 interaction with OH^-, forming CO_3^{2-}, and dendrite formation which further reduces the electrolyte's ionic conductivity and slows the cell's reactions [26], [27], [28], [29]. This degradation limits the number of charge-discharge cycles the battery can undergo before its capacity significantly decreases [11].

Slower Kinetics: ZABs suffer from slower kinetics, particularly in the ORR and OER that occur at the air cathode. These reactions are very slow, leading to high overpotentials and reduced overall efficiency. Enhancing the kinetics of these reactions typically requires the use of expensive catalysts like platinum and other noble metals, which increases the cost and complexity of the batteries [24].

Dendrite Formation: Dendrite formation on the zinc anode is another critical issue. During the charging process, uneven deposition of zinc can lead to the growth of dendritic structures. These dendrites can pierce the separator, causing short circuits and

posing a significant safety risk. Moreover, dendrite formation contributes to the overall degradation of the anode, further limiting the battery's cycle life and reliability [30].

Addressing these challenges requires a comprehensive approach, including the development of more stable and conductive electrolytes, and innovative designs to mitigate dendrite formation. By overcoming these obstacles, ZABs could fulfill their potential as a high-energy-density, cost-effective, and environmentally friendly energy storage solution.

1.3. Importance of Near-Neutral Electrolytes

Near-neutral electrolytes, like $ZnCl_2$ and NH_4Cl used in Leclanché batteries, play a critical role in enhancing performance, safety, and sustainability. These electrolytes, with pH values close to 7, offer several advantages over more acidic or alkaline alternatives.

Firstly, near-neutral electrolytes help to prevent corrosion, extending the lifespan of the battery by providing a stable environment that reduces the risk of material degradation. As it is mentioned in [31], the electrolyte (NH_4Cl) used in the Zn/MnO_2 battery system helps mitigate corrosion by forming a passivation layer composed of ZnO and $Zn(NH_3)_2Cl_2$ on the zinc anode's surface. This layer protects the zinc from further corrosion, thus prolonging the battery's lifespan. Furthermore, concerning performance the near-neutral $ZnCl_2+NH_4Cl$ solution optimizes ion transport, maintaining efficient electrochemical reactions and minimizing unwanted side reactions. This ensures consistent battery capacity and extended shelf life, making the Leclanché battery a dependable option for low-drain applications such as remote controls, clocks, and flashlights.

Lastly, safety is another significant advantage. The near-neutral $ZnCl_2+NH_4Cl$ electrolyte is less dangerous to handle and store compared to extreme pH electrolytes, this helps to reduce the potential for chemical burns and simplifies handling procedures. This safety aspect is particularly beneficial for consumer applications where ease of use and minimal risk are essential [32].

1.3.1. Issues with CO_2 Interaction and Dendrite Formation

In battery technology, two main problems with near-neutral electrolytes such as $ZnCl_2$+NH_4Cl for Leclanché batteries include interaction with CO_2 and zinc dendrite formation, which can affect battery performance, safety, and longevity.

CO_2 Interaction: Carbon dioxide is common in the environment. This is because it interacts with the electrolyte in Leclanché batteries resulting in various undesired reactions. When it dissolves in a near-neutral $ZnCl_2$+NH_4Cl electrolyte, it forms carbonic acid (H_2CO_3) which may then dissociate into hydrogen ions (H^+) and bicarbonate ions (HCO_3^-). During such reactions, the pH value of the electrolyte can become depressed thereby reducing it from its near-neutral condition to an acidic medium. Furthermore, the bicarbonate ions present can cause the anode to develop as zinc carbonate ($ZnCO_3$). At the beginning, this passivation layer protects, but it may occur as too heavy leading to lower zinc ions (Zn^{2+}) transference as well as reducing battery effectiveness [33].

Dendrite Formation: A critical issue in near-neutral electrolyte-containing zinc batteries is dendrite formation. Dendrites in this context are zinc structures that are needle-like in appearance and grow on the positive electrode (cathode) when a battery is being charged. When zinc ions undergo a reduction and are deposited on the electrode, they may deposit in a nonuniform manner especially under high current densities due to cycling for a long time. In this sense, we will highlight 3 main troubles that arise due to the expansion of zinc dendrites:

1. Short Circuits: Sometimes dendrites reach the cathode after growing long enough to pierce through the separator; as a result, there is an internal short circuit. Such cases may lead to an immediate battery collapse, heat up, or even combustion.

2. Decreased effectiveness: Due to the formation of dendrites, zinc is unevenly deposited hence decreasing the surface area of the anode that is effective for electrochemical reactions. Over time, this non-uniformity may decrease the battery's total efficiency as well as its capacity.

3. Dendrites emerging leads to the breach of the separator and other battery compartments thus undermining the stability of the battery as a whole.

Several strategies can be used to prevent dendrite formation. These include improving the electrolyte composition to encourage more consistent zinc deposition, the use of additives that hinder dendrite growth, and making advanced separators, which can physically obstruct such formations [34].

1.4. Historical and Contemporary Electrolytes

The evolution of electrolytes in battery technology has been marked by significant advancements, driven by the need for improved performance, safety, and sustainability. This section outlines the historical development of electrolytes and the contemporary innovations that have shaped modern battery systems.
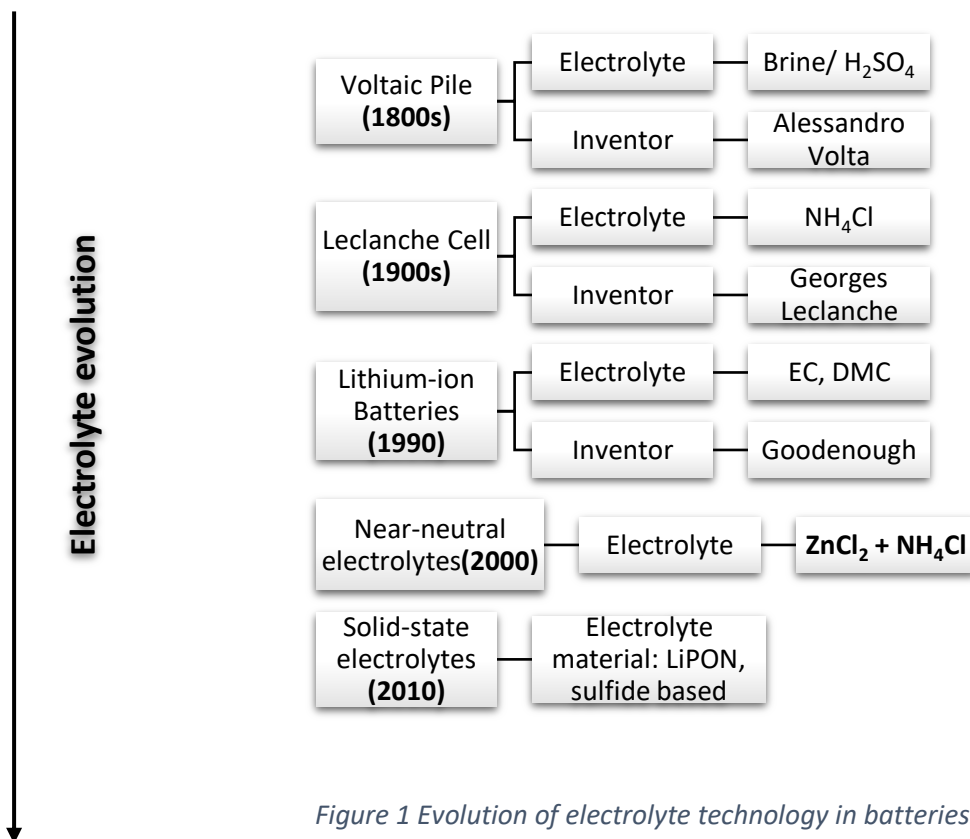
Figure 1 Evolution of electrolyte technology in batteries.

Figure 1, illustrates the evolution of electrolyte technology in batteries from the early 1800s to the present day, highlighting key developments and innovations in electrolyte materials and their inventors.

Historical background on electrolytes Alessandro Volta invented the voltaic pile or the earliest battery in 1800, he did that by employing sulfuric acid and brine as electrolytes. These simple aqueous electrolytes allowed the ions to move from electrode to electrode

and that made it possible for electricity generation. But despite their efficiency, they were very hazardous because they used dangerous elements like corrosive sulfuric acid and brine [35].

In the late 19th century, the Leclanché cell utilized an electrolyte comprising NH_4Cl, which was less corrosive than sulfuric acid. Due to this reason, it lasted longer and was safer for general applications/usage [36].

During the mid-20th century, alkaline batteries were made. Unlike the electrolytes before, these batteries overcame most of the challenges associated with their predecessors. KOH was used as one of its alkaline electrolytes and offered mostly higher power densities than those ever realized before and up to now has longer life expectance in terms of storage duration than any other kind. As a consequence, such batteries were soon implemented into consumer electronics given that they were supported by ion transport that is stable and effective in an alkaline medium. However, the high corrosiveness of alkaline electrolytes required careful material selection and design to prevent leakage and degradation [37].

Contemporary electrolytes: In the last half-century, efforts have been directed to the creation of electrolytes that balance high performance with safety as well as environmental sustainability. In line with this development, there has been a move towards the adoption of near-neutral electrolytes such as those found in today's zinc-based batteries. As an illustration, the contemporary Leclanché batteries use an electrolyte containing $ZnCl_2$ and NH_4Cl, representing great strides made over conventional electrolytes due to low corrosivity advantages [38]. The creation of non-aqueous and solid-state electrolytes has been another breakthrough in the modern-day electrolyte realm. Organic solvents play a crucial part in today's portable electronics and electric vehicle market with lithium-ion batteries as the main source that employ them like ethylene carbonate (EC) or dimethyl carbonate (DMC) as electrolytes [39]. Despite their high voltage stability and energy density, non-aqueous electrolytes suffer from risks such as flammability as well as electrolyte degradation.

Solid-state electrolytes are under intensive research and development to overcome lots of restrictions met in liquid electrolytes. One of the ways to do this is by removing liquid electrolytes, instead using a solid material that can be used in batteries hence providing increased energy storage capacities. This will also make safer batteries with increased life spans as opposed to the reverse being the case if things remained unchanged. Some of the solid electrolyte materials include lithium phosphorus oxynitride (LiPON) and sulphide-based electrolytes, which are considered to be the most favourable ones for making a solid-state battery that can store more energy than any other batteries [40], [41], [42].

1.4.1. $ZnCl_2$–NH_4Cl as Electrolyte

Aqueous $ZnSO_4$ and $ZnCl_2$ electrolytes are frequently employed in industrial zinc electroplating processes. These weakly acidic solutions offer nearly 100% coulombic efficiency for zinc electrodeposition [43]. Considering their high electrical conductivity, sulphate- and chloride-based electrolytes are ideal for secondary zinc battery applications. Studies show that zinc batteries using these electrolytes can reliably function for hundreds to thousands of cycles [44]. However, maintaining a near-neutral pH requires a buffer solution to offset the effects of oxygen-reduction and oxygen-evolution reactions. For $ZnCl_2$, this is achieved by adding NH_4Cl and NH_4OH. The state of aqueous zinc ions in buffered electrolytes and the solubility of solid precipitates at near-neutral pH is very complex [43], [45], [46]. A detailed understanding of the electrolyte's composition and its behaviour during cell operation is essential for developing a practical battery. The $ZnCl_2$–NH_4Cl system has been used in commercial electrochemical systems since the 19th century, serving as the standard electrolyte for zinc-carbon (Leclanché) batteries [3]. In this sense, a major research topic in the development of Leclanché batteries is understanding how electrolyte composition affects performance and capacity. Studies have shown that at low NH_4Cl concentrations (less than 10 wt%), the discharge product is amorphous zinc chloride hydroxide monohydrate (Simonkolleite: $ZnCl_2 \cdot 4Zn(OH)_2 \cdot H_2O$). In contrast, higher NH_4Cl concentrations result in crystalline zinc diammine chloride ($ZnCl_2 \cdot 2NH_3$) as the solid product [47], [48]. It is also suggested that due to its crystallization morphology, $ZnCl_2 \cdot 2NH_3$ poses a higher risk of passivation than $ZnCl_2 \cdot 4Zn(OH)_2 \cdot H_2O$ [49]. Unlike alkaline zinc batteries, there is no

standard formulation for the Leclanché electrolyte. The $ZnCl_2/NH_4Cl$ ratio is adjusted based on the specific battery application. Today, $ZnCl_2$–NH_4Cl has mostly been replaced by KOH in zinc-carbon batteries due to its higher conductivity. However, the ongoing search for alternatives to lithium-based energy storage technologies has renewed interest in neutral zinc-air batteries. This is because the use of cheap and non-hazardous materials, along with the potential for high energy density, makes zinc-air batteries a promising contender for sustainable stationary energy storage [50].

1.4.2. Comparison with KOH

ZABs are being explored as alternatives to conventional lithium-ion batteries due to their cost-effectiveness, safety, and environmental friendliness. The electrolyte used in these batteries significantly influences their performance, stability, and overall efficiency. While KOH is typically used as the electrolyte in ZABs, it also presents some drawbacks. To understand the comparative performance of the $ZnCl_2+NH_4Cl$ electrolyte system with KOH electrolytes, key factors such as ionic conductivity, current density, and biodegradability are discussed. The ionic conductivity of electrolytes is a critical factor for battery performance. KOH electrolytes exhibit high ionic conductivity, typically ranging from 500 to 600 mS/cm, which enhances efficient ion transport and improves battery efficiency. Conversely, $ZnCl_2+NH_4Cl$ electrolytes have lower conductivities, around 100 to 150 mS/cm, which can limit their performance in high-power applications [51]. Current density is another important factor affecting the battery's ability to deliver power. KOH electrolytes can support higher current densities, up to 200 mA/cm², due to their superior conductivity [51], while $ZnCl_2+NH_4Cl$ electrolytes support lower current densities, up to 100 mA/cm², which may affect the battery's power output and recharge rate [52]. Both electrolyte systems exhibit similar specific capacities when using zinc as the anode material, with values around 820 mAh/g. This high specific capacity is beneficial for achieving high energy density in zinc-based batteries [51]. KOH electrolytes provide high electrochemical stability but are prone to issues such as CO_2 absorption, leading to the formation of potassium carbonate, which reduces the electrolyte's effectiveness over time. $ZnCl_2+NH_4Cl$ electrolytes, while less conductive, offer stable performance in near-neutral pH conditions, reducing the risk of side reactions and maintaining long-term stability [49], [51], [53]. $ZnCl_2+NH_4Cl$ electrolytes

are generally safer and more environmentally friendly compared to KOH electrolytes. KOH is highly corrosive and poses significant handling and environmental risks, whereas $ZnCl_2+NH_4Cl$ is less corrosive, making it a preferable choice for applications where safety and environmental impact are critical concerns [52].

In conclusion, KOH electrolytes, with high ionic conductivity (500-600 mS/cm) and the ability to support high current densities (up to 200 mA/cm²), are ideal for high-power applications in zinc-based batteries. However, they are highly corrosive, absorb CO_2, and pose environmental risks. In contrast, $ZnCl_2+NH_4Cl$ electrolytes have lower conductivity (100-150 mS/cm) and support lower current densities (up to 100 mA/cm²), but offer greater stability in near-neutral pH conditions, reducing side reactions and maintaining long-term effectiveness. They are also less corrosive and more environmentally friendly, making them a safer and more sustainable option for applications where environmental impact and safety are critical.

1.5.   Polymer Gel-Based Electrolytes

Electrolytes are essential components in batteries, enhancing the movement of ions between the cathode and anode. A polymer electrolyte can be generally defined as a membrane that exhibits transport properties comparable to those of typical liquid ionic solutions. Polymer electrolytes were first introduced by Fenton in 1973 [54], and the development of polymer electrolytes has progressed through three distinct stages: (i) dry solid-state polymers, (ii) gel/plasticized polymer electrolyte systems, and (iii) polymer composites [55]. The earliest example of a "dry solid" polymer electrolyte corresponds to the poly (ethylene oxide) (PEO) based system, which demonstrated very low ambient temperature conductivities of around 10^{-8} S.cm^{-1} [54]. In such system, the polymer host serves as a solid solvent without any organic liquid. However, its cycling performance with lithium metal electrodes was unsatisfactory, achieving only 200-300 cycles. This poor performance was attributed to the low ionic conductivity of the electrolytes. The second category of polymer electrolytes is known as "gel polymer electrolytes" or "plasticized polymer electrolytes." These systems are characterized by their unique state, which is neither fully liquid nor solid, but rather a combination of both states [56], [57]. In this sense, a gel polymer electrolyte (GPE) combines the

properties of both solid and liquid electrolytes. It consists of a polymer matrix that is swollen with a liquid electrolyte solution. The polymer matrix provides mechanical stability and flexibility, while the ionic solutions offer high ionic conductivity. This semi-solid structure minimizes the risks associated with leakage and flammability, making gel electrolytes safer and more suitable for a wide range of battery applications, including flexible and wearable electronics. Moreover, GPE also helps to suppress dendrite formation, enhancing the electrochemical stability and cycle life of batteries [58]. However, the practical application of GPEs in rechargeable zinc-air batteries (RZABs) remains challenging due to several issues. The poor solubility of zinc salts in GPEs, coupled with the high viscosity and flammability of organic solvents such as DMSO, ethylene carbonate, and propylene carbonate, make these electrolytes unsuitable for use in zinc-air batteries, which are open systems [59]. Common polymer matrices for GPEs include poly (ethylene oxide) (PEO), poly (vinyl chloride) (PVC), poly (methyl methacrylate) (PMMA), poly (vinylidene fluoride-hexafluoropropylene) (PVDF-HFP), poly (vinylidene fluoride) (PVDF), poly (acrylic acid) (PAA), and poly(acrylonitrile) (PAN) [60]. These polymers have been employed as host materials due to their ability to provide mechanical integrity to the GPE structure. Ideal polymer hosts should possess particular properties, such as fast segmented motion of the polymer chain, a wide electrochemical window, high molecular weight, low glass transition temperature, the ability to promote salt dissolution, and high degradation temperature [61].

1.5.1 Gel Polymeric Host Materials for electrolytes in Zinc Air Batteries

In the preparation of GPEs, a host polymer, which acts as the base matrix, is required before the inclusion of any other materials. Commonly used host polymers in GPE preparation include poly (vinyl alcohol) (PVA), poly (vinyl chloride) (PVC), poly (ethylene oxide) (PEO), poly(acrylonitrile) (PAN), poly (acrylic acid) (PAA), poly (ethyl methacrylate) (PEMA), poly (vinylidene fluoride) (PVDF), poly (methyl methacrylate) (PMMA), and poly (vinylidene fluoride-hexafluoropropylene) (PVDF-HFP) [62], [60].

Poly (vinyl alcohol) (PVA): PVA is an excellent host polymer due to its unique properties, including good mechanical strength, cost-effectiveness, tensile strength, optical properties, non-toxicity, excellent film-forming ability, ease of preparation, chemical and thermal stability, flexibility, high abrasion resistance, and biocompatibility. Its

physical properties vary depending on the degree of polymerization and alcoholysis [7]. The presence of numerous functional hydroxyl groups enhances water absorption. Recently, PVA has been examined as a gel electrolyte in ZABs for flexible energy devices due to its promising mechanical characteristics [63].

Poly (acrylic acid) (PAA): PAA is used as a battery binder because of hydrogen bond formation within the carboxyl groups produced by hydroxyl groups. It is a promising host polymer for alkaline electrolytes in ZABs [7] .

Poly (acrylamide-co-acrylic acid) (P-(AM-co-AA)): This copolymer is commonly used as a host in GPEs for planar ZABs. It has improved water retention capacity, superior atmospheric stability, and higher ionic conductivity compared to commonly used alkaline gel electrolytes like PVA [64].

Poly (ethylene oxide) (PEO): PEO is a popular host polymer known for its high capacity in salt complexation, dimensional stability, corrosion resistance, mechanical flexibility, high ionic conductivity in the amorphous state, chemical stability, and reasonable cost [62]. However, its tendency to crystallize at lower temperatures limits its ionic conductivity at ambient temperature, making it less effective as a host polymer [60].

1.5.2 Advantages of Gel Polymer Electrolytes over Liquid-State Electrolytes

GPEs offer several advantages over traditional liquid-state electrolytes in battery applications, particularly in ZABs. These advantages include improved safety, enhanced mechanical properties, better electrochemical stability, and versatility and customization. One of the most outstanding advantages of GPEs is their safety improvements. Traditional liquid electrolytes are at risk of leakages, leading to possible short circuits and fires. In contrast, GPEs have a semi-solid structure that reduces the possibility of leakages, hence lowering the chances of a complete breakdown. Therefore, GPEs are highly recommended for use in flexible and wearable electronic devices due to their enhanced safety profile. The semi-solidity of GPEs brings outstanding mechanical properties such as flexibility and toughness, which are crucial for wearable gadgets and flexible electronics. The polymer matrix in GPEs helps maintain the shape of the electrolyte when subjected to mechanical strains, making them suitable for applications where the battery needs to bend or stretch without compromising efficiency.

Additionally, GPEs exhibit greater electrochemical stability compared to liquid electrolytes. They are less prone to the formation of dendrites, which are needle-like structures that can grow in the electrolyte and cause short circuits. The polymer matrix in GPEs inhibits dendrite formation, resulting in longer battery life and more dependable operations. Furthermore, GPEs offer versatility and customization, as they can be easily tailored by incorporating different polymers and additives to achieve desired properties. This flexibility enables the adjustment of the electrolyte to suit specific applications, such as increasing ionic conductivity, enhancing thermal stability, or improving mechanical strength. The ability to customize GPEs makes them an attractive option for a wide range of energy storage applications [7].

GPEs offer several advantages over traditional liquid-state electrolytes in battery applications, particularly in ZABs. These advantages include improved safety, enhanced mechanical properties, and better electrochemical stability. Therefore, the most outstanding advantages that gel-state electrolytes exhibit when compared to conventional liquid electrolytes are safety improvements, enhanced mechanical properties, improved electrochemical stability, and versatility and customization.

Safety Improvements: The safety profile of batteries is highly boosted by GPEs. Traditional liquid electrolytes are at risk of leakages, hence possible short circuits and fires. In contrast, GPEs have a semi-solid structure that reduces the possibility of leakages occurring, hence lowering the chances of a complete breakdown. Therefore, they are highly recommended for use in flexible and wearable electronic devices given that there is a need for them to be safe [65].

Enhanced Mechanical Properties: The semi-solidity of GPEs brings outstanding properties like flexibility and toughness. Flexibility is termed so important in wearable gadgets, and flexible electronics because of the need to bend/stretch the battery without compromising on its efficiency. Also, the polymer matrix in GPEs helps to maintain the shape of the electrolyte when it is subject to mechanical strains [66].

Improved Electrochemical Stability: Greater electrochemical stability is exhibited by GPEs relative to liquid electrolytes. It is unlikely for them to have dendrites formed since they are less prone to needle-like structures growing in the electrolyte. In GPEs, the

polymer matrix serves to inhibit the formation of dendrites, which in turn means a longer battery life as well as more dependable operations [67].

Versatility and Customization: GPEs can be easily customized by incorporating different polymers and additives to achieve desired properties. This flexibility enables adjustment of the electrolyte to suit particular uses, such as increasing ionic conductivity, enhancing thermal stability, or improving mechanical strength. The ability to tailor the properties of GPEs makes them an attractive option for a wide range of energy storage applications [68], [69], [70].

1.5.3 Polymer Electrolytes (PEs) and Their Challenges

In recent times, PEs have become crucial in enhancing the efficiency and safety of ZABs by increasing ionic mobility, mechanical stability, and electrochemical potential. However, several issues hinder their full exploitation in real-life applications. One key challenge is achieving high ionic conductivity, which is crucial for effective performance in ZABs. The ionic conductivity is influenced by factors such as the degree of crystallinity, polymer chain mobility, and the polymer's ability to solvate ions. Enhancing this property often involves optimizing the polymer structure and incorporating additives that facilitate ion transport [71]. Another significant challenge is the mechanical stability of PEs, which is essential for maintaining the battery's structural integrity under various operating conditions, including resistance to deformation and maintaining contact with the electrodes. Therefore, developing polymers that offer a balance between flexibility and strength is key [72]. Furthermore, PEs must be chemically stable to prevent reactions with other battery components, and thermally stable to withstand the operational temperatures of the battery. Lastly, for polymer electrolytes to be commercially viable, they must be cost-effective and easy to produce on a large scale. This involves developing manufacturing processes that are economical and environmentally friendly [64].

1.6   Biopolymeric Electrolytes

Biopolymeric electrolytes have gained significant attention in recent years due to their potential for sustainability and environmental friendliness. These materials, derived from natural sources, offer unique properties that make them suitable for various

electrochemical applications, including batteries [73]. Biopolymeric electrolytes, such as those made from chitosan, cellulose, and alginate, possess excellent biocompatibility, biodegradability, and mechanical properties. These polymers can form hydrogels, which are three-dimensional networks capable of retaining large amounts of water, making them ideal for use in GPEs. The natural abundance and sustainability of these materials further enhance their appeal for use in energy storage devices [7], [74], [75]. The synthesis of biopolymeric GPEs involves various gelation methods, including physical and chemical crosslinking. Techniques such as solution casting, electrostatic association, and phase inversion are commonly employed to form gel structures. The choice of method depends on the specific biopolymer and the desired properties of the final electrolyte [7]. Biopolymeric electrolytes have shown promise in ZABs, offering improved ionic conductivity and stability. For instance, chitosan and cellulose-based GPEs have been extensively studied for their ability to enhance the performance of ZABs. These materials provide a stable matrix that can effectively retain electrolytes and facilitate ion transport, which is crucial for the efficient operation of these batteries [7].

1.6.1 Chitosan and Starch-Based Hydrogels

Chitosan and starch-based hydrogels are two such materials with great promise for electrolytes in several electrochemical applications. These natural-polymer-based hydrogels are characterized by unique properties, among which high ionic conductivity, biocompatibility, and environmental friendliness present them as candidates for energy storage devices, sensors, and other electrochemical systems.

Moreover, these hydrogels are bioactive and are made by deacetylating chitin's polysaccharide. It has an excellent film-forming ability, a high mechanical strength, and good ionic conductivity. The hydrogels can be efficiently designed to have tailor-made ionic conductivity and mechanical properties through variation in the degree of deacetylation, along with different cross-linking methods, for example, ionic interactions or covalent bonding. The microstructure of chitosan hydrogels is characterized by a highly porous network that facilitates efficient ion transport. The formation of this porous network is influenced by various crosslinking methods, including, ionic Interactions and covalent bonding. Chitosan molecules contain amino groups that can interact with multivalent ions such as calcium or zinc to form ionic

bonds. These ionic interactions create a stable network that enhances the hydrogel's mechanical strength and ionic conductivity [76]. Furthermore, in covalent bonding**,** chemical crosslinking agents such as glutaraldehyde, genipin, or carbodiimides can be used to form covalent bonds between chitosan chains. Covalent crosslinking results in a more rigid and durable hydrogel structure, which is crucial for maintaining structural integrity in electrochemical applications [76].

In this sense, starch-based hydrogels with excellent ionic conductivity will make their use as an electrolyte material in producing batteries, supercapacitors, and fuel cells possible. The hydrogel's porous structure allows for effective ion transport, while its biocompatible and biodegradable nature makes it friendly toward affordable energy storage solutions. Furthermore, starch-based hydrogels can be doped with various ionic salts to enhance their electrochemical performance, making them versatile materials for a wide range of electrochemical devices.

1.6.2 Potential in Energy Storage Technologies of Hydrogels

Hydrogels are considered one of attractive materials for use as electrolytes in many energy storage devices because of their unique properties, high ionic conductivity, mechanical strength, and environmental-friendly.

Table 1 summarizes different hydrogel-based electrolytes with some of the main primary materials, battery applications, performance in batteries, electrochemical properties, and references of critical studies. The information was collected from a mix of recent research covering all-starch-based hydrogels, CMC-CS hydrogels, and other biopolymer hydrogel electrolytes, showing the potential and advances in energy storage technologies.

Table 1. Overview of hydrogel-based electrolytes for energy storage applications.

Hydrogel name	Primary materials	Battery application	Performance in batteries	Electrochemical properties	Ref.
All-Starch-Based Hydrogel	High-amylose starch, $CaCl_2$, glycerol	Zn-Cu batteries	Demonstrates a voltage of 0.81 V; high sensitivity to compression	Efficient ion transport and mechanical stability under compression.	[77]

CMC-CS Hydrogel	Chitosan, Carboxymethylc ellulose (CMC), Citric Acid	ZABs	Enhanced ionic conductivity (0.39 S/cm) due to pores and channels from crosslinking strategies; maximum power density of 117 mW/cm² and specific capacitance of 1899 mAh/g	Arrhenius conduction mechanism from 0°C to 70°C; cation transport mechanism associated with ion jumping to nearest vacant sites, resulting in thermally assisted ionic conductivity.	[78]
Biopolymer Hydrogel Electrolytes	Chitosan, PVA, Polyacrylamide	ZABs, Supercapa-citors	Improved ionic conductivity and mechanical stability; high flexibility and biocompatibility.	High electrochemical stability; effective ion transport at various temperatures.	[79]
Flexible Hydrogel Electrolytes	Various biopolymers, crosslinkers	Flexible and wearable batteries	High tensile strength, freeze-tolerance, enhanced mass transport.	Suppression of dendrite formation, stable performance over multiple cycles.	[80]
Cellulose-Based Hydrogels	Cellulose, Ionic liquids	Energy storage devices, supercapa-citors	High mechanical strength, and environmental friendliness.	Good ionic conductivity, effective at various temperatures.	[81]

1.7 Operational Dynamics of Zinc-Air Batteries with Near-Neutral Gel Polymer Electrolyte

Understanding the performance of these materials in practical applications, such as the operational dynamics of ZABs, is crucial. Thus, this research explores the operational dynamics of a ZAB using a $ZnCl_2$–NH_4Cl ionic solution within a GPE matrix (Figure 2). This analysis is critical for elucidating the electrochemical performance and stability of the system. A battery prototype was developed consisting of a metallic Zn electrode and a porous gas-diffusion electrode (GDE) loaded with a bifunctional air catalyst (Pt/C), based on configuration reported in [82]. The GPE separates the electrodes and conducts ions across the cell. During discharge, the zinc metal electrode undergoes a reaction where

it dissolves into aqueous Zn^{2+} ions (Equation 12), which then potentially form complexes with other species present in the solution.

$$Zn \leftrightarrows Zn^{2+}2e^-, E^0 = -0.762V \qquad \textbf{\textit{Eq. 12}}$$

When zinc solubility limit is surpassed, solids like ZnO, Zn (OH)$_2$, ZnCl$_2$·4Zn(OH)$_2$·H$_2$O, and ZnCl$_2$·2NH$_3$ start to precipitate. The literature states that the ratio of NH$_4$Cl concentration in the electrolyte determines the type of discharge product formed. For instance; low concentrations (e.g., less than 10 wt%) would enhance the precipitation of amorphous ZnCl$_2$·4Zn(OH)$_2$·H$_2$O (Simonkolleite), whereas high concentrations of NH$_4$Cl promote the formation of crystalline ZnCl$_2$·2NH$_3$, which poses a greater risk of passivation [83]. During discharging, oxygen gas enters through the gas diffusion electrode (GDE) and dissolves in the gel, where it undergoes reduction catalysed by a bifunctional catalyst to form water as indicated in Equation 13:

$$0.5O_2^{aq} + 2H^+ + 2e^- \rightleftharpoons H_2O, E^0 = 1.229V \qquad \textbf{\textit{Eq.13}}$$

This reaction involves the consumption of protons, varying the NH$_4^+$/NH$_3$ equilibrium and triggering the buffer reaction to stabilize the pH within the gel. However, zinc ions will form complexes with NH$_3$ and Cl$^-$, depending on the local pH and ion concentrations (e.g ZnCl$_x$ (NH$_3$)$_y^{n-}$, Zn(NH$_3$)$_4^{2-}$), thus displacing the equilibrium of NH$_4^+$ to the right-hand side to replenish the loss of NH$_3$ (Equation 14).

$$NH_4^+ \rightleftharpoons NH_3 + H^+ \qquad \textbf{\textit{Eq. 14}}$$

The GPE setup enhances these processes by providing a stable matrix that minimizes unwanted precipitates, facilitating smoother transitions and better handling of the electrochemical products, particularly favouring ZnO formation over less desirable chlorine-containing compounds. Furthermore, it is important to mention the electrolyte's capacity to maintain a neutral pH largely stems from the interaction between ZnCl$_2$ and NH$_4$Cl. The NH$_4^+$/NH$_3$ buffer reaches its equivalence point at a pH of 9.8 [84]. In a pure NH$_4$Cl solution, pH stabilization is temporary, as rising NH$_3$ concentrations soon make the solution alkaline. However, when NH$_4$Cl is combined with ZnCl$_2$, Zn^{2+} ions bind with NH$_3$ to form complexes stable within a pH range of about 6–

10. These zinc-ammine complexes help absorb free NH_3 (Equation 15), enhancing the buffer's effectiveness in maintaining a neutral pH.

$$Zn^{2+} + nNH_3 \rightleftharpoons Zn(NH_3)_n{}^{2+}$$

Eq. 15

Therefore, the importance of combining both $ZnCl_2$ with NH_4Cl. Nevertheless, when transitioning to ZABs with neutral electrolytes, a key distinction is observed: unlike the stable pH maintained by strongly alkaline KOH electrolytes in typical setups, the near-neutral pH in $ZnCl_2$-NH_4Cl electrolytes shifts with minor pH changes. This variability significantly influences the dominant zinc complexes, affecting the physicochemical properties and the electrolyte's buffering capacity [50]. This complex understanding of zinc stability under varying pH levels is essential for optimizing ZAB performance and reliability.

Considering the above, this research aims to explore the electrolytic behaviour of chitosan-starch-based biopolymeric hydrogels in quasi-neutral ionic solutions within a $ZnCl_2$+ NH_4Cl system. The impact of pH variation on the structure, morphology, thermal, mechanical, and electrochemical properties of the membranes was evaluated, alongside the performance of the electrolyte without the inclusion of the membrane. Primary battery tests were performed to measure the apparent resistance, power density, and specific capacity of the cell prototypes developed in this research. The proposed combination of GPE with pH-stabilizing ionic solutions promises to enhance the viability and efficiency of these innovative energy systems.

Figure 2. Operational Diagram of a zinc-air battery with ZnCl₂-NH₄Cl electrolyte, illustrating various electrochemical reactions within the cell, different colours and shapes that depict no specific significance have been used. Black arrows highlight the flow of these reactions as they occur during the battery's discharging phase (Adapted from [50]*).*

Chapter 2: Problem Statement and Objectives

2.1 Problem Statement

In the pursuit of green innovation, the development of sustainable, cost-effective, and high energy-density electrochemical storage devices is paramount [85] . ZABs emerge as a highly promising candidate in the energy storage domain due to their exceptional energy density relative to their size and weight. Despite these advantages, the widespread adoption of ZABs is hindered by their limited cycle life and sluggish kinetics, critical parameters for rapid discharge and recharge capabilities essential in industrial applications [25]. Moreover, atmospheric exposure introduces CO_2, which reacts with OH^- ions, leading to the formation of CO_3^{2-}, and dendritic structures. These phenomena significantly diminish the ionic conductivity of the electrolyte and impede the efficiency of electrochemical reactions within the cell [26], [27], [28], [29]. On the contrary, maintaining the electrolyte around at a near-neutral pH mitigates the formation of CO_3^{2-}, preserving ionic conductivity, enhancing electrochemical reaction efficiency, and improving the cyclic stability of the battery [86], [87], [88]. This approach leverages current chemical understanding and builds upon the historical evolution of electrolytes such as $ZnCl_2$-NH_4Cl (pH stabilizing solution), traditionally used in electrochemical systems, especially in zinc-carbon batteries, also known as Leclanché cells [89], [90], [91].

A critical factor in the development of these eco-friendly batteries is the physical state of the electrolyte. Currently, batteries are composed of liquid electrolytes, which have drawbacks including safety risks, toxicity, flammability, potential leakage, bulky design, electrode corrosion at interfaces, and dendrite growth on metal electrodes, ultimately constraining their capacity and lifespan [92], [93]. In response to these problems, modern battery development strategies are oriented towards the use of solid or gel-based electrolytes to improve their electrochemical properties. Among the various solid-state and gel-based electrolytes, polymer electrolytes (PEs) have garnered considerable attention for their remarkable flexibility and reliable performance [94], [95]. Nevertheless, PEs face challenges such as low efficiency, limited ionic conductivities, and

insufficient electrochemical stability [7], [96]. Due to these limitations, recent trends in research advocate for the integration of organic and inorganic components, resulting in hybrids with superior mechanical strength, enhanced ionic conductivity, and non-flammable systems.

Current research into gel polymer electrolytes (GPE) specifically explores pH adjustments of the $ZnCl_2$-NH_4Cl ionic solution within these hybrids to optimize their performance across various applications, aligning with the overarching objective of improving electrochemical stability and environmental sustainability [97], [98], [99]. Based on the advances in GPEs the search for sustainable energy storage technologies continues to drive research in the development of new materials. Among these materials, biopolymer electrolytes derived from renewable resources such as chitosan and starch are promising hybrid alternatives. Their biocompatibility, affordability, and customization make them especially attractive for environmentally sensitive applications, pushing the boundaries of energy storage technology [100], [101], [102].

Considering the mentioned, this research aims to explore the electrolytic behaviour of chitosan-starch-based biopolymeric hydrogels in quasi-neutral ionic solutions within a $ZnCl_2$+ NH_4Cl system. The impact of pH variation on the structure, morphology, thermal, mechanical, and electrochemical properties of the membranes was evaluated, alongside the performance of the electrolyte without the inclusion of the membrane. Primary battery tests were performed to measure the apparent resistance, power density, and specific capacity of the cell prototypes developed in this research. The proposed combination of GPE with pH-stabilizing ionic solutions promises to enhance the viability and efficiency of these innovative energy systems.
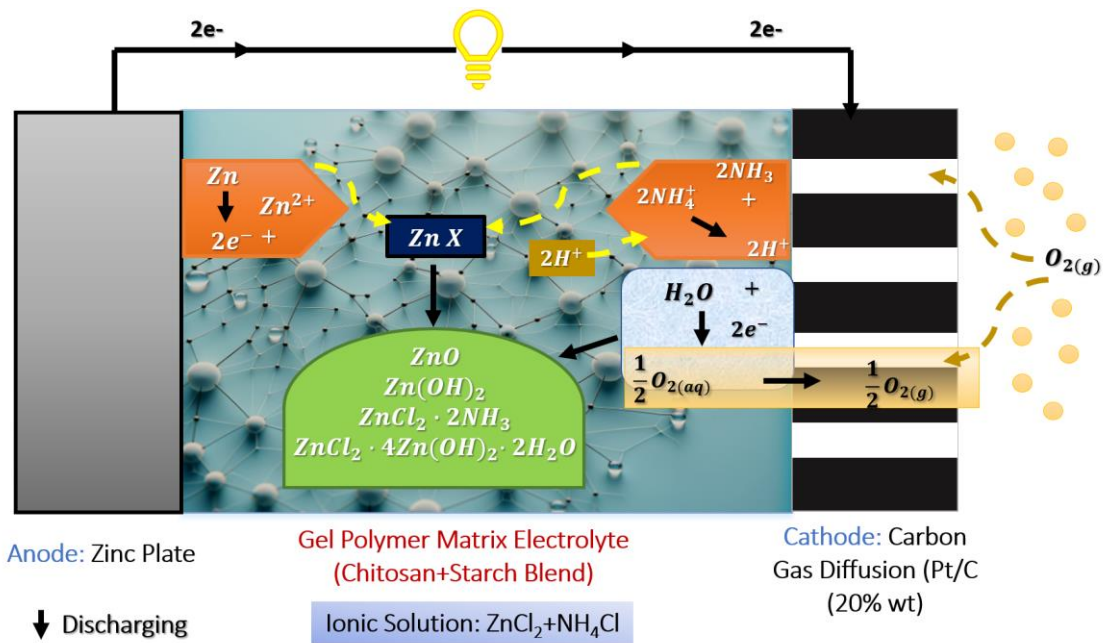
2.1.2 General Objective

To develop and characterize biopolymeric electrolytes based on chitosan and starch embedded in different concentrations of $ZnCl_2$+NH_4Cl ionic solution, whilst varying the pH from 4, 6 up to 7. In this sense, this project aims to explore near-neutral eco-friendly, and sustainable alternatives to conventional liquid electrolytes, with a focus on enhancing the electrochemical performance and safety of primary ZABs.

2.1.2 Specific Objectives

To thoroughly investigate the properties and performance of biopolymeric electrolytes embedded in near-neutral ionic solutions for use in ZABs, this project has specific objectives described according to the different stages of the experimental procedure.

1. **Synthesis of Chitosan-Starch Hydrogels:**

- To develop biopolymeric electrolytes using a combination of food-grade chitosan and starch as base materials for the polymeric matrix which will be the host for the $ZnCl_2$-NH_4Cl ionic solution, which will be evaluated in a ZAB prototype.

2. **Morphological and Structural Characterization:**

- To apply Fourier-transform infrared spectroscopy (FTIR) to examine the molecular structure and functional groups of the GPEs before and after discharge tests, noting changes due to immersion in varying pH ionic solutions.
- To perform X-ray diffraction (XRD) to identify solid products influenced by different pH values in the ionic solutions, and to investigate how these products affect the crystal structure, crystallinity, and ionic conductivity of the GPEs.
- To conduct thermogravimetric analysis (TGA) to assess the thermal stability and decomposition behaviour of the biopolymeric electrolytes from room temperature to 800 °C.
- To evaluate the swelling ratio and absorption capacity, determining the liquid retention capabilities of the synthesized GPEs after 24 hours of immersion in different ionic solutions with pH adjustments ranging from 4 to 7.

3. **Electrochemical Performance and Immersion Studies:**

- To assess the effect of ionic solution concentration and varying pH on the ionic conductivity using electrochemical impedance spectroscopy (EIS) across temperatures from 0 °C to 50 °C.
- To evaluate the impact of immersion in $ZnCl_2$ + NH_4Cl solutions with 0.51 M $ZnCl_2$ and varying NH_4Cl concentrations (1.6 M and 2.34 M) at pH 4, 6, and 7 on the electrochemical performance and stability of GPEs, focusing on current density, specific capacity, and overall ZAB prototype performance.

Chapter 3: Methodology

3.1 Materials and Chemicals

In this study, high-purity food-grade chitosan (90.6% deacetylated [103], BioFitnest, 100% purity) was employed. The starch used in the experiments was obtained from Sigma Aldrich. The ionic solution components, $ZnCl_2$, NH_4Cl, and NH_4OH (diluted solutions at 10% and 5%), were also sourced from Sigma-Aldrich. Distilled water was employed as the solvent for all solutions. For the electrochemical testing, platinum plates (99.97% purity) and zinc discs (99.999% purity) were obtained from Goodfellow. The battery experiments used SIGRACET® 39 B slides, measuring 10 mm in width, 15 mm in length, and 0.4 mm in thickness, for the cathode. These slides were coated with a commercial catalytic ink containing Pt/C at a catalyst mass loading of 1 mg.cm^{-2}. The anode was fabricated from high-purity zinc foil (99.99% purity, Yunexpress Inc., Shenzhen, China), with dimensions of 10 mm in width, 15 mm in length, and 0.2 mm in thickness.

3.1.1 Preparation of Ionic Solutions: Formulation and pH

The ionic solutions were meticulously prepared by dissolving NH_4Cl and $ZnCl_2$ in water. The pH of the resulting solutions was finely tuned by incrementally adding NH_4OH, (concentration based on the study [104]) in with precise adjustments made to achieve the targeted pH levels, as detailed in, Table 2.

Table 2. Formulation and pH Adjustment of ZnCl$_2$-NH$_4$Cl Ionic Solutions.

Electrolyte name	ZnCl$_2$ (M)	NH$_4$Cl (M)	NH$_4$OH (M)	pH	Ref.
M_pH 4	0.51	1.60	1×10^{-3}	4	[105]
M_pH 6	0.51	2.34	0.22	6	[105],[106]
M_pH 7	0.51	1.60	0.76	7	[106], [44]

3.1.2 Synthesis of Chitosan-Starch Hydrogels

The hydrogels were synthesized using the lyophilization method in a 3-step synthesis procedure (following the scheme previously reported in [102]. In this sense, the

hydrogel synthesis started with dissolving chitosan (CS) and starch (AS) separately and then mixing them into a homogenous solution, (Figure 3). Epichlorohydrin (5% wt.) was added for cross-linking, followed by ultrasound and stove treatments to facilitate structural transformations. An additional step was included to control membrane thickness, utilizing a 3:3 polymer ratio. Controlled volumes of the mixture were placed in Petri dishes to achieve a desired thickness of 2.5 mm after a 48 -hour lyophilization process, which also removed excess moisture.

The molar concentration of the ionic solution of 0.51M $ZnCl_2$+2.34M NH_4Cl used in this study was based on the models reported in [105], [106], and the electrolyte composition of 0.51M $ZnCl_2$+1.6M NH_4Cl was based on the studies in [104], [106]. The pH range values were chosen based on the findings of the dominant aqueous zinc complexes and discharge product solubilities for a total chlorine concentration of 3.36M reported in [105]. In this sense, NH_4OH pH adjusting solutions were prepared according to the concentrations stated in Table 2, and adjusting the pH was performed under rigorous tracking with the help of a pH meter HANNAH pH edge model. Consequently, the synthesized polymer membranes were immersed in the following ionic solutions: 0.51M $ZnCl_2$ + 1.6M NH_4Cl (pH= 4), 0.51M $ZnCl_2$ + 2.34M NH_4Cl (pH= 6), 0.51M $ZnCl_2$ + 1.6M NH_4Cl (pH= 7), during 24 h prior to structural and electrochemical characterization procedures. The NH_4Cl ratio was changed to evaluate its influence on the discharge product. Furthermore, to elucidate the advantages of incorporating membranes, the liquid electrolyte was assessed in the absence of membranes during the discharge tests in the battery prototype. To facilitate a comprehensive understanding of the results obtained in this study, specific codes were designated to identify the membranes treated at various pH levels and their corresponding chemical electrolytes, as detailed in Table 3 and Table 4.

Table 3. Sample codification based on pH variations for membranes.

Ionic Solution	Measured pH	Hydrogel Code
0.51M $ZnCl_2$- 1.6M NH_4Cl	4	M_pH 4
0.51M $ZnCl_2$- 2.34M NH_4Cl	6	M_ pH 6
0.51M $ZnCl_2$ – 1.6M NH_4Cl	7	M_ pH 7

Table 4. Sample codification based on pH variations for liquid electrolytes.

Ionic Solution	Measured pH	Electrolyte Code
0.51M $ZnCl_2$- 1.6M NH_4Cl	4	L_pH 4
0.51M $ZnCl_2$- 2.34M NH_4Cl	6	L_ pH 6
0.51M $ZnCl_2$ – 1.6M NH_4Cl	7	L_ pH 7
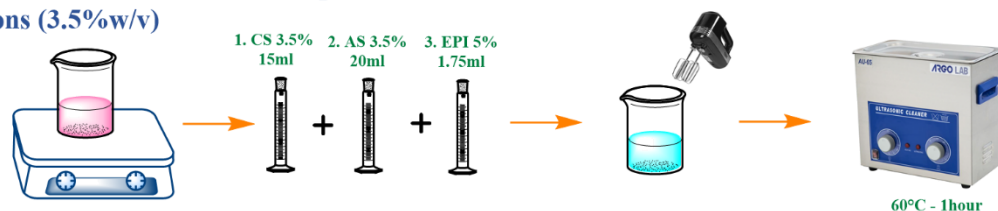
Figure 3. Synthesis of chitosan-starch hydrogels using physical crosslinking techniques.

3.2 Morphological and Structural Analysis

Fourier Transform Infrared (FTIR) spectroscopy in the solid state was used with attenuated total reflectance (ATR) mode to analyse the effect of the ionic solution's pH on the functional group changes within the polymer matrices. Hence, FTIR was performed both before and after discharge tests to evaluate the microstructural changes. In this manner, Spectra were acquired using a Cary 630 spectrophotometer (Agilent Technologies Inc., Santa Clara, CA, USA) equipped with a single-bounce Diamond ATR accessory. The spectra were recorded over the range of 4000–400 cm^{-1}, with 64 scans and a resolution of 4 cm^{-1}.

The thermal properties of the gel polymer electrolytes were assessed through thermogravimetric analysis (TGA) utilizing a DSC-TGA Q600 instrument (TA Instruments,

New Castle, DE, USA). The analysis was conducted over a temperature range from ambient to 800 °C, with a controlled heating rate of 10 °C/min under N_2 atmosphere.

Surface micrographs were obtained using scanning electron microscopy (SEM) using a JEOL JSM6010/LV microscope (JEOL Ltd., Tokyo, Japan). Prior to imaging, the samples were dried in a muffle furnace at 60°C for 1 day to remove excess moisture. Elemental analysis was performed on the swollen samples as well as on those utilized in battery prototypes, employing energy-dispersive X-ray spectroscopy (EDX). The EDX analysis was performed using an integrated EDX TEAM system within the SEM apparatus.

X-ray diffraction (XRD) was used to study the influence of pH adjustments and NH_4Cl concentrations on the crystalline structures present. X-ray diffractograms were obtained using a computer-controlled Rigaku Mini-flex-600 (Rigaku, Tokyo, Japan). Measurements were performed with a D/tex Ultra 2 detector. The X-ray generator was placed in a sealed tube with a Ni-filtered Cu Kα radiation source (15 mA, 40 kV, λ = 0.15418 nm). The chosen angular region was 2θ = 5°–70°, with a step width of 0.010°. Match! Software version 3 [107], was employed to identify the characteristic peaks of the crystalline structures of the ionic solution $ZnCl_2+NH_4Cl$.

For swelling ratio (SR) calculations, the samples were weighed before and after 24 h of being immersed in the different ionic solutions. After that, the SR was determined using Equation 16:

$$SR = \frac{W_S - W_0}{W_0} \times 100\% \quad \textit{Eq.16}$$

where, **W** represents the volume or weight, and the subindexes **S** and **0** refer to the swollen hydrogel and the dry electrolyte, respectively.

3.3 Electrochemical Experiment

3.3.1 Electrochemical Impedance Spectroscopy and Cyclic Voltammetry

Electrochemical measurements were performed using electrochemical impedance spectroscopy (EIS) with a VIONIC instrument (Metrohm model, Ecuador). In this sense, EIS was conducted over a frequency range spanning from 100 kHz to 1 Hz. This

measurement setup featured two Pt plates that housed the electrolyte within a cell configuration, with each Pt electrode having a 1 cm² surface area, acting as blocking electrodes. Furthermore, the relationship between ionic conductivity and temperature was performed by employing a Julabo (-40 °C, 15 L) R-temperature control system, obtained from Polyscience, within the temperature range of 0 °C to 50 °C with a remarkable ±1 °C precision. After a 4-minute stabilization period, ionic conductivity (σ) was calculated using Equation 17, (as explained in [108]).

$$\sigma = \frac{l}{A*R_b} \quad \textbf{\textit{Eq.17}}$$

In equation (14), *A* represents the Pt plate area, *l* is the thickness of the gel polymer electrolyte (GPE), and R_b is the bulk resistance, extracted from the intersections of the Nyquist curve with the x-axis. Impedance measurements were conducted up to 4 cycles for each GPE. Moreover, the activation energy (E_a) for each electrolyte was determined using the Arrhenius Equation 18 through linear fitting, where the relationship between ln(σ) and 1000/T was plotted:

$$\sigma = \sigma_0 \exp\left[-\frac{E_a}{K_b(T)}\right] \quad \textbf{\textit{Eq.18}}$$

Here, K_b signifies Boltzmann's constant, σ_0 is a pre-exponential factor, and T represents the absolute temperature.

Cyclic voltammetry (CV) measurements were conducted using a symmetrical two-electrode Zn/hydrogel/Zn cell with 0.5 cm² non-blocking Zn discs. The measurements were performed at a sweep rate of 50 mV·s⁻¹ over a symmetrical potential range from −1.5 V to +1.5 V.

3.2.2 Electrode Cleaning Procedure

For the cyclic voltammetry (CV) experiments, the zinc electrodes underwent a two-step polishing and rinsing procedure. Initially, the electrodes were polished using 600-grit sandpaper, followed by sequential rinsing in distilled water, ethanol, methanol, and finally Type 1 distilled water. After the first polishing cycle, the electrodes were further polished with 1200-grit sandpaper and rinsed again in the same order: distilled water,

ethanol, methanol, and Type 1 distilled water. This ensured a clean and smooth surface for the experiment.

For the Electrochemical Impedance Spectroscopy (EIS) experiments, platinum electrodes, being more delicate, were polished with 1200-grit sandpaper from the start to avoid any damage or scratches. After polishing, the electrodes were rinsed in the following order: distilled water, ethanol, methanol, and finally Type 1 distilled water. This careful polishing and rinsing process ensured a clean and smooth surface, suitable for precise EIS measurements.

3.2.3 Activation Energy calculation

The Arrhenius equation is used to describe the temperature dependence of reaction rates. It is expressed as:

$$k = A.\, e^{\frac{E_a}{K_b T}} \quad \textbf{\textit{Eq. 19}}$$

Where:

- **k** is the rate constant,
- **A** is the pre-exponential factor,
- **Ea** is the activation energy,
- **K$_b$** is the Boltzmann's constant,
- **T** is the temperature in Kelvin.

To determine the activation energy (**E$_a$**), we can rearrange the Arrhenius equation (Equation 19) into a linear form suitable for plotting. By taking the natural logarithm of both sides, we get:

$$Ln\left(\frac{k}{A}\right) = \frac{-E_a}{K_b T} \quad \textbf{\textit{Eq. 20}}$$

Applying natural logarithm of both sides of Equation 20 and further simplifying:

$$Ln(k) = \frac{-E_a}{K_b T}.\frac{1}{T} + In(A) \quad \textbf{\textit{Eq.21}}$$

This is in the form of a linear equation $y = mx + b$, where:

- $y = Ln(k)$

- $m = \frac{-E_a}{K_b T}$

- $x = \frac{1}{T}$

- $b = \mathcal{L}n(A)$

By plotting $\mathcal{L}n(k)$ versus $\frac{1}{T}$, the slope m of the line can be used to determine the activation energy. The slope (extracted from the plot) is given by:

$$m = \frac{-E_a}{K_B T} \quad \textbf{\textit{Eq. 22}}$$

From Equation 22, we can solve for the activation energy:

$$E_a = m.\ K_B \quad \textbf{\textit{Eq.23}}$$

with $K_b = 8.617 \times 10^{-5} eV$ the activation energy can be calculated as:

$$E_a = m.\ 8.617 \times 10^{-5} eV\ .k.\ \frac{1000}{k} \quad \textbf{\textit{Eq. 24}}$$

And finally, the activation energy is equal to

$$E_a = m.\ 8.617 \times 10^{-2} eV \quad \textbf{\textit{Eq.25}}$$

3.2.4 Battery Prototye

The battery tests were conducted based on the previous setup [109], using an AMETEK® VersaSTAT 3 potentiostat/galvanostat (Princeton Applied Research, Berwyn, IL, USA), seen in Figure 4. The anode was a piece of polished high-purity Zn foil (15 × 10 mm, 0.2 mm depth, 99.9% purity, Yunexpress Inc., Shenzhen, China). The cathode was a SIGRACET® 39 B slide (15 × 10 mm, 0.4 mm depth) impregnated with commercial catalytic ink and Pt/C (20% wt.) with a catalyst mass loading of 1 mg cm^{-2}. For battery assembly, hydrogels were placed between the electrodes. EIS curves were assessed at the OCP in a frequency range of 100 kHz to 0.1 kHz. For the polarization curves, the discharge current density was 20 mA cm^{-2}, and the cut-off voltage was 0.2 V. The specific capacitance was determined through the zinc weight loss after discharging the Zn–air battery at 1.98 mA cm^{-1}.
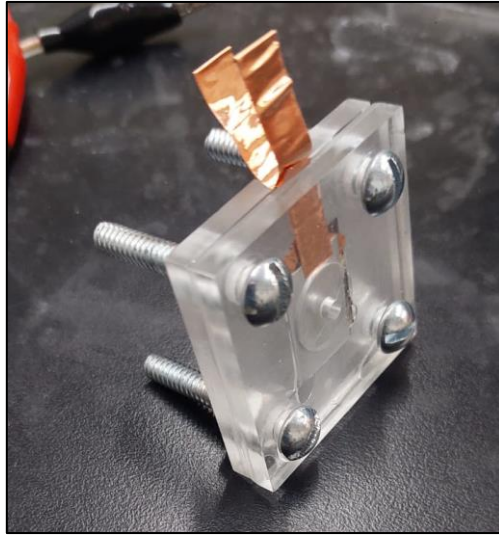
Figure 4. Zinc-air battery prototype with GPEs.

Chapter 4: Results and Discussion

4.1. Physicochemical Characterization.

4.1.1. FTIR analysis before battery discharge test.

The FTIR spectra of both dried and hydrated gel polymeric system are presented in Figure 5. A broad peak observed in all hydrated membranes, within the range of 3200-3600 cm^{-1}, is characteristic of O-H stretching associated with water [110], while N-H stretching from the amine or amide groups in chitosan appears around [111]. The reduced intensity of the O-H vibration in the FTIR spectra can be attributed to the lyophilization (freeze-drying) process. This process removes much of the water content from the hydrogels, which leads to a significant reduction in the number of free hydroxyl (O-H) groups that typically contribute to strong hydrogen bonding [112]. Consequently, the O-H stretching vibrations appear weaker in the spectra. While this reduced intensity is observed across all hydrogels, it is particularly noticeable in the dry membrane, where the absence of water results in minimal O-H signal, as reflected by the lack of distinct peaks in this region. A notable peak at approximately 2871 cm^{-1} corresponding to the symmetric stretching of C-H bonds in methyl (-CH$_3$) and methylene (-CH$_2$-) groups [113]. In the dry membrane, these C-H groups likely adopt a more rigid and ordered conformation, resulting in a more pronounced stretching vibration in the IR spectrum. Conversely, in the hydrated membranes, the presence of water and subsequent formation of hydrogen bonds may mask or shift the C-H vibration, reducing their prominence. Furthermore, in the dried membrane, the peak observed at around 2326 cm^{-1} in the dried membrane suggests the presence of CO$_2$, likely due to atmospheric contamination, as this peak does not correspond to any of the functional groups of chitosan or starch [114]. The absence of this peak in hydrated membranes indicates that CO$_2$ does not play a significant role in the hydrated state or does not affect it similarly to the dry condition. The peak around 1550 cm^{-1} observed in all FTIR spectra (both dry and hydrated membranes) corresponds to the amide II band, which involves N-H bending and C-N stretching in amide groups [113]. This peak is characteristic of the structure of chitosan biopolymer, which contains these functional groups. The consistent presence of this peak at all pH levels suggests that the amine groups remain active and contribute to the hydrogel structure regardless of pH conditions. The peak around 1400 cm^{-1} is commonly due to NH$_2$ bending vibrations in amine groups [111], and

remains relatively stable across the pH levels. In the dry membrane, the amine groups may be less accessible due to the lack of hydration. The absence of water can cause the amine groups to be more compact and less active, resulting in a lower peak intensity. However, this peak may become sharper and more pronounced at higher pH levels, indicating a more pronounced contribution from the C=O stretching as the amine groups are less protonated and thus more available for interaction with Zn^{2+} ions [115]. Near 1020-1080 cm^{-1}, the peaks correspond to C-O stretching vibrations indicative of the glycosidic bonds present in the polysaccharide structures of chitosan and starch. This region appears consistent across all pH levels, suggesting that the glycosidic bond structure remains stable and less affected by the pH changes [116].
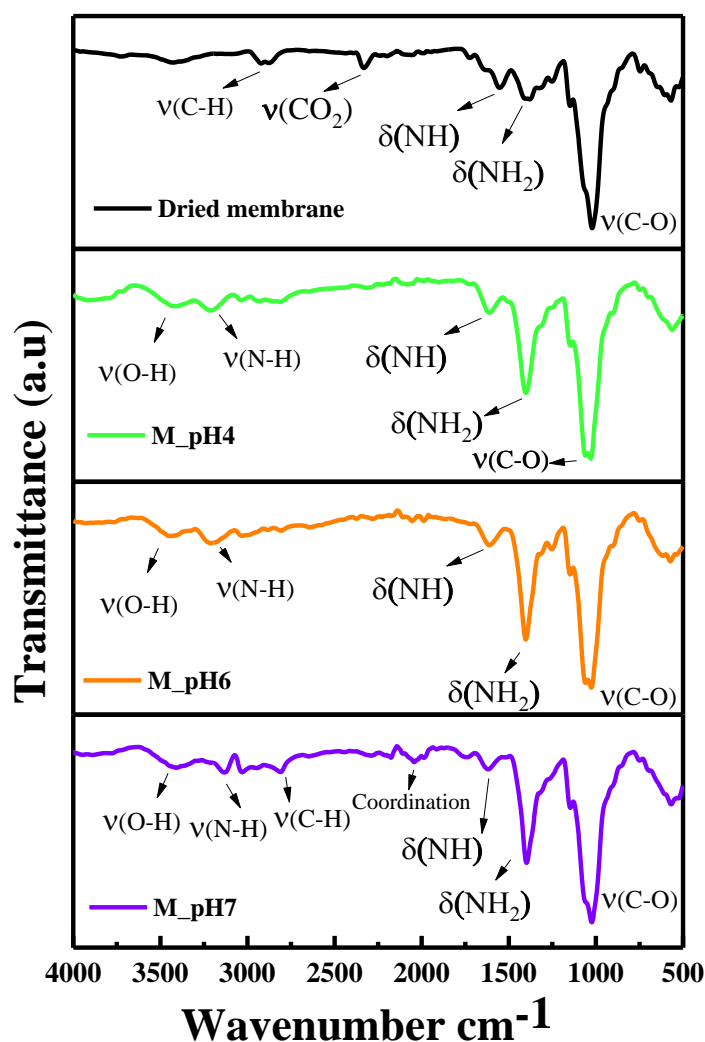

Figure 5. FITR spectra of all GPEs, including dried membrane.

On the other hand, the FTIR spectra from hydrated membranes at different pH values (M_pH4, M_pH6, M_pH7) have provided similar responses, however, there were some minimal microstructural differences found that can be attributed to the pH influence. At pH 4, the acidic environment likely protonates the amine groups, leading to altered interactions with zinc ions from $ZnCl_2$ solution. This protonation reduces hydrogel flexibility and porosity, limiting zinc ion mobility and thereby impacting the hydrogel's ionic conductivity and structural integrity [117], [116],[118]. As the pH increases to 6 and further to 7, the degree of protonation of these groups diminishes. This reduction in protonation is reflected in broader peaks around 3000-3500 cm^{-1} (O-H and N-H stretching) and 1650 cm^{-1} (C=O stretching), due to diminished hydrogen bonding and a higher degree of ionization, suggesting a more flexible hydrogel structure with potentially enhanced ion transport capabilities [116], [118]. Some particular signals are more pronounced at pH 7. The peak at around 2823 cm^{-1} is attributed to the C-H stretching of aldehyde groups (-CHO), [119]. The unique appearance of this peak under these conditions suggests that pH 7 favors a specific conformation or interaction in the hydrogel structure that is not observed at other pH levels. The peak at 2040 cm^{-1} (labeled as "coordination") observed specifically at pH 7 could be due to particular interactions between the functional groups of the hydrogel and the ions present in the solution, stabilizing vibrations that are not observed at other pH levels. In this sense, the presence of peaks at the 2040-2074 cm^{-1} region has been attributed to the formation of ionic coordination complexes [120]. Specifically, these peaks have been observed to correspond to free ions, ion pairs, and ionic aggregates, suggesting a specific interaction between the ions and the functional groups of the polymer.

4.1.2. Thermogravimetric Test

Thermogravimetric Analysis (TGA) of GPEs under various pH conditions to evaluate their thermal stability is an essential factor for boosting battery safety and mitigating the risk of thermal runaway. The initial degradation peaks uniformly observed around 100°C in all samples (Figure 6) can be attributed to the water evaporation. This consistent initial thermal response across different pH levels suggests that the primary phase of thermal degradation remains relatively stable. However, a nuanced analysis reveals that the degree of initial mass loss varies with pH. For instance, the sample at pH 4 exhibits a more gradual and prolonged weight loss, reaching up to 80%. This behaviour implies enhanced water retention or more

stable interactions between water and the polymer matrix, potentially due to increased hydrogen bonding or electrostatic interactions. These findings are supported by previous research [121].

In contrast, the dry matrix shows a more pronounced water loss and faster degradation, which can be explained by the lack of hydration in $ZnCl_2$ and NH_4Cl solutions. The ionic interactions between Zn^{2+} ions and the functional groups in chitosan and starch in the hydrated samples significantly enhance water retention, contributing to greater thermal stability and slower weight loss during TGA. Without these ionic cross-links, the dry matrix experiences more rapid degradation, which explains its more pronounced weight loss during heating [122], [123].

As the temperature increases, samples exposed to higher pH levels (pH 6 and 7) display a pronounced onset of degradation at slightly elevated temperatures compared to the pH 4 sample. This observation suggests that less acidic conditions may afford modest improvements in thermal stability. This hypothesis is supported by the sharper Differential Thermogravimetric (DTG) peaks observed for pH 6 and 7 (Figure 6b), reflecting a more rapid and pronounced decomposition process at these pH levels, with weight losses of 75% and 70% (happening between 200 °C and 350 °C), respectively. In contrast, the pH 4 sample shows a broader and less defined DTG peak, corresponding to a total weight loss of 80%. Residual weight data above 400°C further indicate that higher pH samples exhibit slightly lower residual weights, implying that interactions between the polymer and ions in the solution may affect structural integrity and the formation of residual char. This phenomenon aligns with findings from [124] and [125], highlighting the altered stability of the polysaccharide backbone and the critical impact of pH on the degradation pathways of these biopolymers. Notably, the M_pH 7 sample exhibits an earlier and sharper second degradation peak, which along with the "Dry matrix" sample showing 60% total weight loss, emphasizes the intricate role of pH in determining the thermal and structural behaviour of biopolymeric electrolytes. This understanding is crucial for advancing the development of safer and high-performance battery technologies.
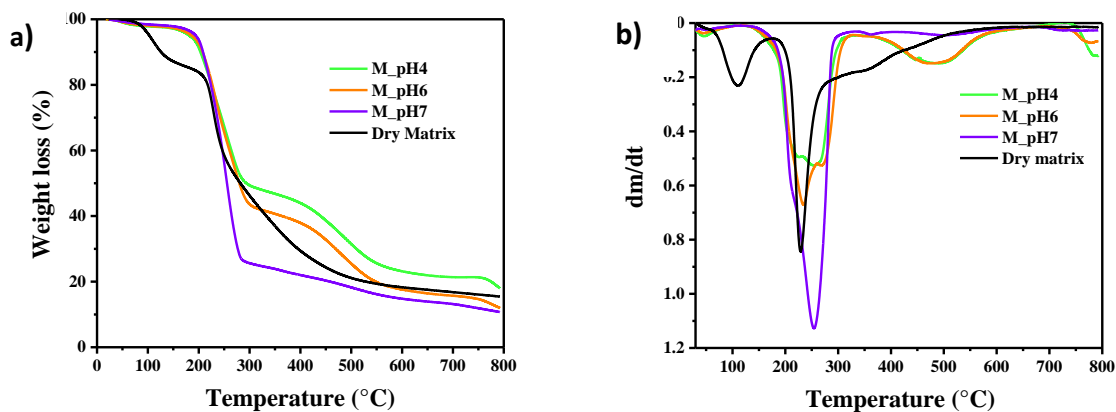
Figure 6. The curves depicting the thermal behaviour of dry and gel polymeric electrolytes at various pH values (a) TGA (b) DGTA curves.

4.2. Structural Analysis before Discharge Battery Test

4.2.1. X-ray diffraction Analysis

The XRD analysis revealed that the nature and concentration of zinc compounds vary significantly with the pH of the electrolyte (Figure 7). The peaks were identified with Match! software database for phase identification. Notable diffraction peaks were observed at 15.3°, 17.5°, and 29.8°. This phase, forms under acidic conditions where NH_3 availability is limited, leading to complexation with Zn^{2+} ions. The presence of $ZnCl_2 \cdot 2NH_3$ suggests that the gel matrix is relatively unstable due to the reduced availability of NH_3. Moreover, the formation of $ZnCl_2 \cdot 4Zn(OH)_2 \cdot H_2O$ is confirmed by peaks observed around 11.37°, 18.2°, and 36.5°, indicating a significant amount of Simonkolleite. Peaks associated with NH_4Cl are also evident at 23.07°, 32.92°, 52.87°, and 58.62°, highlighting the complexity of the precipitate formation at this pH.

In contrast, at pH 6, high-intensity peaks revealed that the predominant solid precipitate corresponds to $ZnCl_2 \cdot 2NH_3$. Peaks of moderate intensity are observed at 15.32° and 17.47°, however, these peaks are intense when compared to pH4's. Furthermore, the characteristic peaks from NH_4Cl salt were also observed at this pH. These results are consistent with the thermodynamic stability diagrams reported in [126], where both pH 4 and pH 6 formulations reach the solubility limit of the chlorinated zinc hydroxide compound. Additionally, the pH 4 electrolyte is further from the solubility limit, allowing a higher percentage of zinc to dissolve

in the electrolyte compared to pH 6. The Simonkolleite compound, $ZnCl_2 \cdot 4Zn(OH)_2 \cdot H_2O$, consumes chloride ions from the electrolyte, affecting the equilibrium of dissolved species and potentially destabilizing the buffering effect of the electrolytic systems.

At pH 7, XRD patterns revealed a clear absence of the $ZnCl_2 \cdot 4Zn(OH)_2 \cdot H_2O$ and $ZnCl_2 \cdot 2NH_3$ which is consistent with the thermodynamic stability diagrams in [126]. This can be particularly beneficial as the products that have precipitated during the discharge process would be not completely redissolved and deposited as Zn metal. Therefore, the dissolution of the precipitated zinc products is suppressed during the discharge process, which could represent significant consequences for the battery reversibility [104]. Hence, the absence of solid precipitates like Simonkolleite or $ZnCl_2 \cdot 2NH_3$ is advantageous for maintaining the efficiency and stability of the electrolyte system.
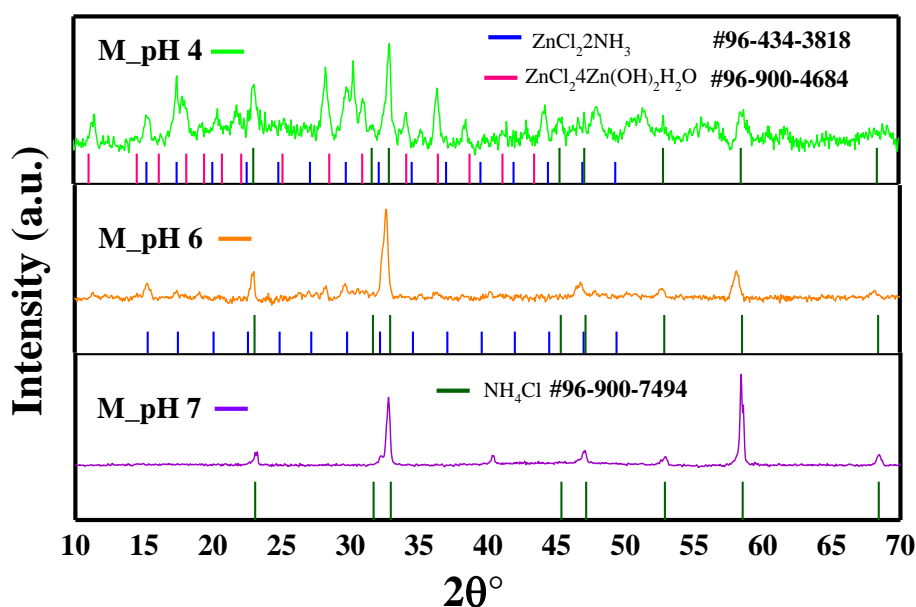

Figure 7. X-ray Diffraction Pattern of the Gel Polymer Electrolyte (GPE) at different pH values.

4.2.3. Scanning Electronic Microscopy

In the scanning electron microscopy (SEM) analysis, distinct microstructural variations emerge between the dry chitosan-starch membrane (Figure 9a), and polymer electrolytes

reported in previous studies, such as those detailed in [127]. These differences are predominantly attributed to the lyophilization parameters employed. For the chitosan-starch membrane, lyophilization was performed using a smaller container with a reduced volume of polymer solution. This methodological adjustment was critical for achieving a controlled gel polymeric electrolyte matrix thickness and a specific structural profile. The rapid freezing conditions imposed in this setup resulted in the formation of smaller ice crystals, leading to more textured and fragmented surface morphology, consistent with observations in [127]. Conversely, the CH: A 1 hydrogel (composed of a mix of chitosan and starch hydrated in 12M KOH) discussed in [127], processed under less restrictive volume conditions, displayed a markedly smoother and more homogeneous structure with well-defined pore architecture. This contrast underscores the impact of lyophilization conditions on the microstructural characteristics of polymer electrolytes, highlighting how variations in freezing rates and solution volumes can significantly influence the resulting surface morphology and porosity of biopolymeric hydrogels.

Moreover, it is important to note that the drying process performed prior to SEM analysis, particularly at 60 °C for 1 day, might have also contributed to the observed microstructural changes in the dry membrane. The dehydration of the sample could have resulted in some contraction and potential collapse of the gel structure, further accentuating the textured and fragmented appearance

The SEM micrograph of the hydrated membrane is shown in (Figure 9b). The hydrogels surface appears smoother and more homogenous, which is indicative of the polymer chains becoming more flexible and increased swelling.

Additionally, Energy Dispersive X-ray Spectroscopy (EDS) was performed, (Figure 10) to determine the overall elemental composition of the dry membrane and the hydrated membrane with $ZnCl_2$+NH_4Cl ionic solution. The appearance of N, Cl, and Zn in the hydrated membrane signifies that the ions from $ZnCl_2$ and NH_4Cl are absorbed and integrated into the membrane matrix.
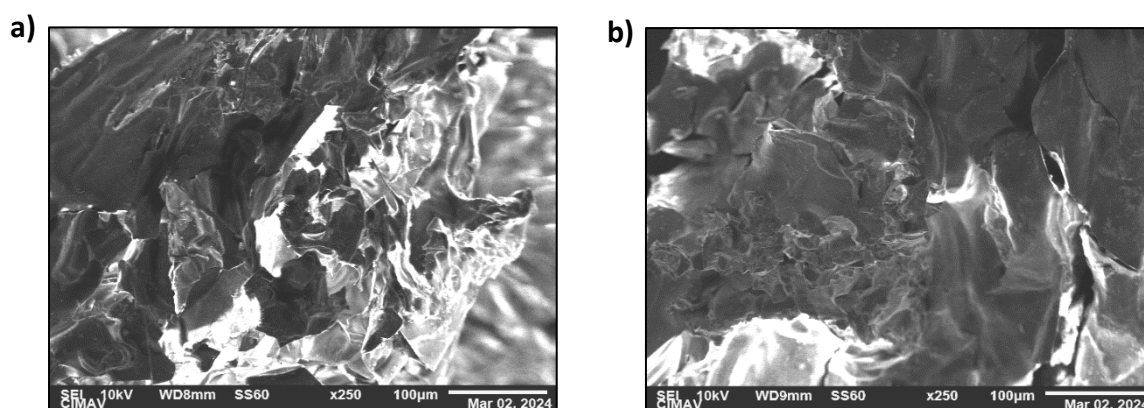
Figure 9. Micrographs of GPEs (a) Dried membrane (b) Hydrated membrane.
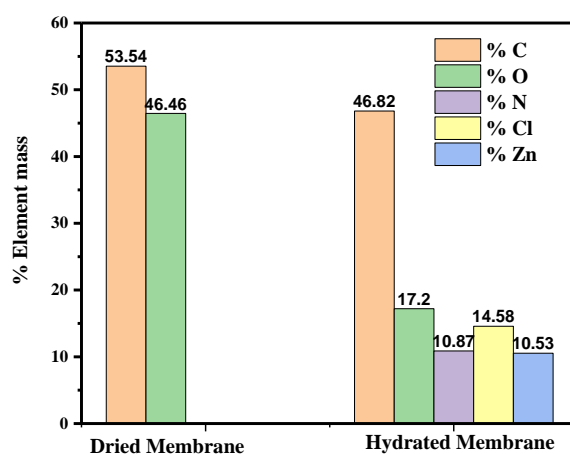
Figure 10. Elemental composition of dry membrane and hydrated membrane.

4.3 Electrochemical Characterization

To characterize the electrochemical performance of all GPEs before the battery test, EIS tests were performed at a temperature range of 0 °C to 50 °C. Furthermore, the swelling ratio (SR) was calculated according to Equation 5. Moreover, to assess the reversibility of GPEs, cyclic voltammetry tests were performed.

4.3.1. Ionic Conductivity and Swelling Degree Evaluation

The ionic conductivity was evaluated with the swelling degree of the GPEs (Figure 11a). It can be acknowledged that both conductivity and absorption increase with the pH level of the GPE, suggesting that a more neutral pH (moving from pH 4 to pH 7) enhanced the gel's ability to

conduct ions and absorb ionic solution (the absorption increased from around 600% to 1300% respectively, aligning with a volume change up to 107%, (Table 5).

Table 5. Ionic solution retention of GPEs.

Electrolyte code	Dried volume (cm^3)	Hydrated volume (cm^3)	Dried weight	Hydrated weight	% Absorption	% Volume change
M_pH4	0.1918	0.3189	0.0248	0.1882	658.9	66.27
M_pH6	0.1963	0.3534	0.0255	0.2588	914.9	80.03
M_pH7	0.1961	0.4059	0.0277	0.6010	1335	107.0

Additionally (Figure 11b) and Table 6 underscore the ionic conductivities (σ) and activation energies (E$_a$) for GPEs at pH 7, pH 6, and pH 4, measured from 0 °C up to 50 °C. The gel polymer electrolyte at pH 7 exhibited the highest ionic conductivity of 0.11 S·cm^{-1} at room temperature (30 °C), combined with the relatively low bulk resistance (5.11 Ω) obtained from EIS measurements, further indicates efficient ion transport and good electrode-electrolyte contact. This lower bulk resistance suggests minimal impedance at the electrode interface, ensuring better overall electrochemical performance. Moreover, the lowest activation energy of 0.075 eV obtained from GPE at pH of 7, suggests that ions move more freely at this pH level, requiring less energy to conduct [128]. This value of 0.11 S.cm^{-1} is notably higher than the conductivities reported in other studies listed in Table 7. For instance, the ZnCl$_2$/NH$_4$Cl PVA-based GPE showed a conductivity of 0.0021 S.cm^{-1} [129], and the PVA-MC-NH$_4$Cl electrolyte reported a conductivity of 1.99 x 10^{-3} S.cm^{-1} [130] . Comparatively, the electrolyte at pH 6 has a lower conductivity of 0.07 S.cm^{-1} and a higher activation energy of 0.144 eV, indicating a reduced ion mobility relative to pH 7. The electrolyte at pH 4 exhibited the lowest conductivity, 0.04 S.cm^{-1}, and an activation energy of 0.128 eV, reflecting the more challenging environment for ion conduction at this acidic pH. These differences affirm the trend observed in the Arrhenius behaviour graph; as the pH becomes more acidic, both the ionic conductivity decreases and the activation energy for ion conduction generally increases, likely due to less favourable conditions for ion transport, such as increased hydrogen bonding or interaction with hydronium ions [57].
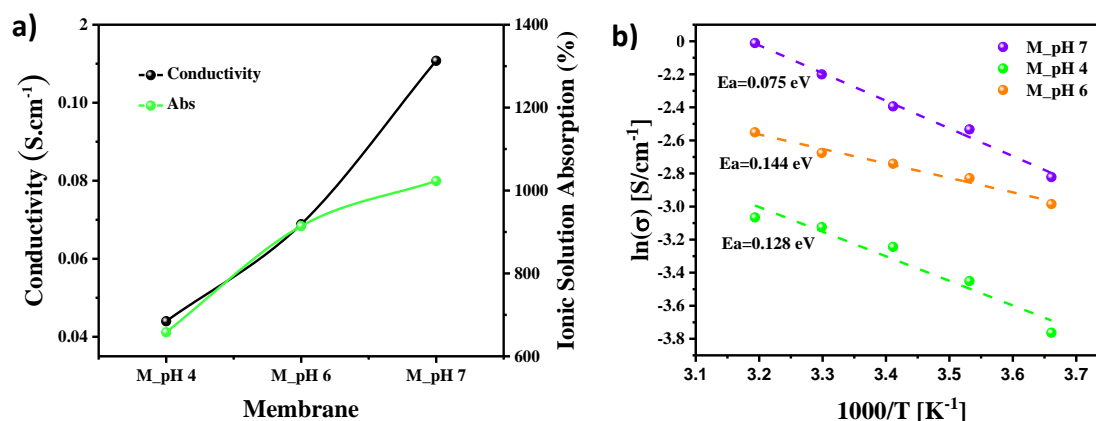
Figure 11. Evaluation of ionic conductivity of GPEs at different pH values (a) Measured ionic conductivity at 30°C versus swelling ratios of GPEs. (b) Ionic conductivity and activation energies of GPEs at the temperature range 0°C to 50°C.

Table 6. Electrochemical values and battery information for the GPEs and liquid electrolytes.

Electrolyte Code	σ (S·cm^{-1})	Ea (eV)	Bulk Resistance (Ω)	Specific Capacitance (mAh.g^{-1})	Power Density (mW.cm^{-2})	Current Density (mA.cm^{-2})
M_pH 7	0.11	0.075	5.11	675	38	130
M_pH 6	0.07	0.144	6.18	342	19	30
M_pH 4	0.04	0.128	2.36	184	16	50
L_pH 7	-	-	4.4	724	11	21
L_pH 6	-	-	7.5	418	1.8	7.9
L_pH 4	-	-	8.1	410	2	11

Table 7. Battery performance of some gel polymer ZnCl$_2$+NH$_4$Cl electrolyte for ZABs.

Electrolyte	Polymer matrix	Salt concentration	σ (S.cm^{-1})	Bulk resistance (Ω)	Specific capacitance (mAh.g^{-1})	Power density (mW.cm^{-2})	Ref.
ZnCl$_2$-HPG	Hydroponics Gel (HPG) made from poly (acrylic acid)	3 M ZnCl$_2$ and 7M NH$_4$Cl	0.026-0.104	25.4-19.8	8.8	12.7-12.2	[52]
ZnCl$_2$/NH$_4$Cl PVA-based GPE	Polyvinyl Alcohol (PVA)	0.6 M ZnCl$_2$ + 2.8 M NH$_4$Cl	0.0021	-	200	15.3	[129]
PVA-ZnCl$_2$ (60:40)	Polyvinyl Alcohol (PVA	40 wt% ZnCl$_2$	3.919 x 10^{-7}	-	-	-	[131]

PVA-MC-NH$_4$Cl	Polyvinyl Alcohol (PVA) and Methyl Cellulose (MC)	50 wt% NH$_4$Cl	1.99×10^{-3}	-	5.5	-	[130]
Chitosan + Starch-ZnCl$_2$+NH$_4$Cl	Chitosan + Starch	0.51M ZnCl$_2$+ 1.6M NH$_4$Cl, pH = 7	0.11	5.11	675	38	This work

4.3.2. Cyclic Voltammetry

The cyclic voltammetry (CV) of near-neutral chitosan-starch-based hydrogels was analysed to evaluate their electrochemical activity in a zinc-air battery (Figure 12). The CV response transitions from a rectangular shape to a sharp leaf shape. Moreover, the lack of distinct redox peaks in the CV curves indicates that the primary charge storage mechanism is electrostatic, with minimal contribution from faradaic reactions, which is crucial for maintaining the cycle stability of ZABs [127]. Nevertheless, in the context of near-neutral electrolytes, the high Lattice Energy (LE) at 708 KJ/mol, of NH$_4$Cl means that the ions do not dissociate as easily, thus contributing primarily to the formation of a double layer of charges rather than undergoing faradaic (redox) reactions [130]. This is why the CV curves show quasi-rectangular shapes indicative of capacitive behaviour, with minimal contribution from faradaic processes. Consequently, the absence of distinct oxidation and reduction peaks in the CV curves is consistent with the presence of a high LE salt like NH$_4$Cl, which limits the availability of free ions for redox reactions. However, in practical ZAB applications, both capacitive and faradaic processes can coexist. This combination of processes allows the battery to exhibit good performance during discharge tests and electrochemical impedance spectroscopy (EIS), despite the primarily capacitive behaviour observed in CV. In this sense, the coexistence of capacitive and faradaic processes in ZABs is made possible by the dual charge storage mechanisms of the electrode materials, the nature of practical battery operations involving redox reactions, and the complementary benefits of high-power density from capacitive storage and high energy density from faradaic reactions [132], [133], [134].

Hence, the CV curves for the hydrogels in different pH environments (pH 4, pH 6, and pH 7) showed minimal differences in current density. However, we can highlight that at pH 7 some early signs of a reduction peak were seen. The stability of the CV curves within a wide potential window (-1.5 V to 1.5 V) suggests that these hydrogels can operate effectively under

standard battery conditions without significant long-term stability and efficiency losses. Furthermore, the highest current density observed for the hydrogel at pH 7, close to 200 mA·cm⁻², confirms its very stable performance in cycling tests. These results collectively support the use of chitosan-starch hydrogels embedded in near-neutral ionic solutions for ZABs, and have demonstrated their high ionic conductivity, capacitive behaviour, and electrochemical stability, all of which are crucial for efficient and reliable operation in energy storage devices.
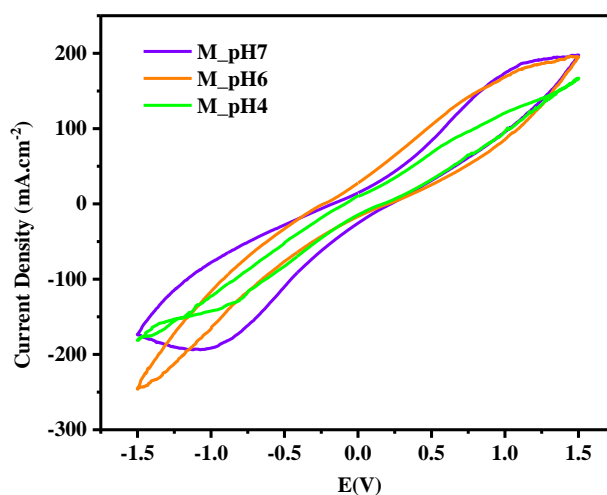
Figure 12. Cyclic voltammograms of GPEs at different pH values.

4.4. Battery Test

The Open Circuit Potential (OCP) of the batteries varied from 1.18 V and 1.4 V for the gel polymeric electrolyte systems, whereas for the only liquid electrolytes went from 1 V to 1.3 V, thus suggesting a more stable and efficient electrochemical potential in the gel system. From the Nyquist plots (Figure 13) bulk resistances for both systems (liquid and membrane) varied from 2Ω to 8 Ω, these low values suggest that the battery has good contact between the electrolyte and the electrodes, which is crucial for efficient ion transport.
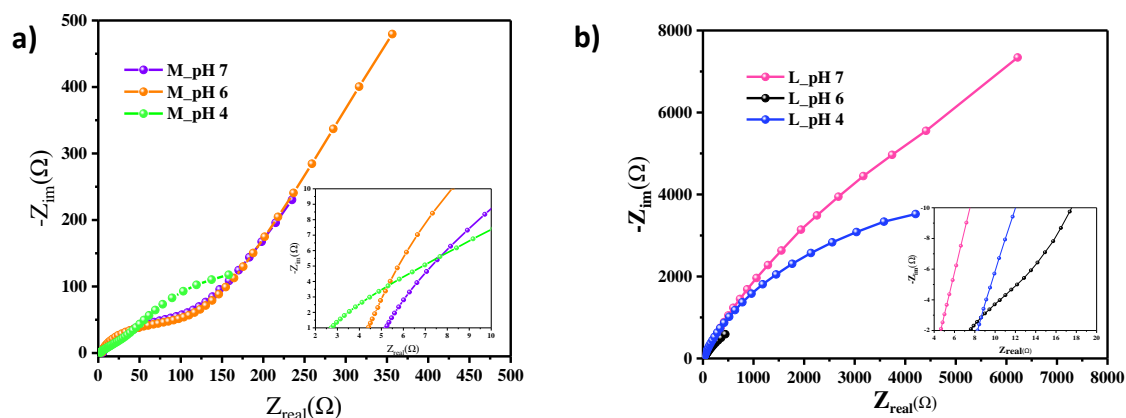
Figure 13. EIS studies of electrolytes in the ZAB prototype. (a) GPE system. (b) Liquid system.

On the other hand, the discharge polarization curves, (current densities and power densities) are displayed in (Figure 14). GPEs (Figure 14c and d), exhibited significantly higher as well as outstanding power densities than their liquid counterparts' electrolytes, with increases of over three times at pH 7, approximately 9.5 times at pH 6, and nearly 9 times at pH 4, highlighting their superior efficiency in maintaining ion pathways under varying pH conditions. In this sense, the highest power density is observed at a near neutral pH of 7 (38 mW.cm^{-2} for M_pH 7) much higher than that reported in literature where maximum power density for a gel polymeric electrolyte system immersed in the ionic solution mixture of $ZnCl_2$+NH_4Cl reached 9-15 mW·cm^{-2} [135], [136], [137]. Furthermore, as the pH decreased to 6 and 4, a notable decline in power density is observed in both gel and liquid electrolyte systems (Figure 14b), underscoring how acidic conditions adversely affect battery performance. This trend is especially significant in liquid electrolytes, where the power density at pH 7 peaks at 11 mW.cm^{-2} but drastically falls to 2 mW.cm^{-2} and 1.8 mW.cm^{-2} at pH 6 and pH 4, respectively. These changes highlighted the increased ohmic losses due to higher resistance and reduced ion mobility in more acidic environments. Moreover, at higher pH values, liquid electrolytes are prone to precipitating white $Zn(OH)_2$ [138], which forms crystalline structures that can obstruct ionic mobility, enhancing internal resistance and enhancing ohmic losses [139]. On the other hand, gel polymeric electrolytes, have potentially provided a more stable ionic pathway. This gel matrix, being viscoelastic, integrates more orderly with electrode materials, avoiding interface detachment issues, thus maintaining lower internal resistance and enhancing overall electrochemical performance [140]. The robustness of these composite hydrogels also helps to prevent issues like water

decomposition and dendrite growth, further stabilizing the battery system under various pH conditions [141]. These attributes make the gel systems less susceptible to the steep voltage declines observed in liquid electrolytes, especially at lower pH levels, leading to a more consistent and improved battery operation.
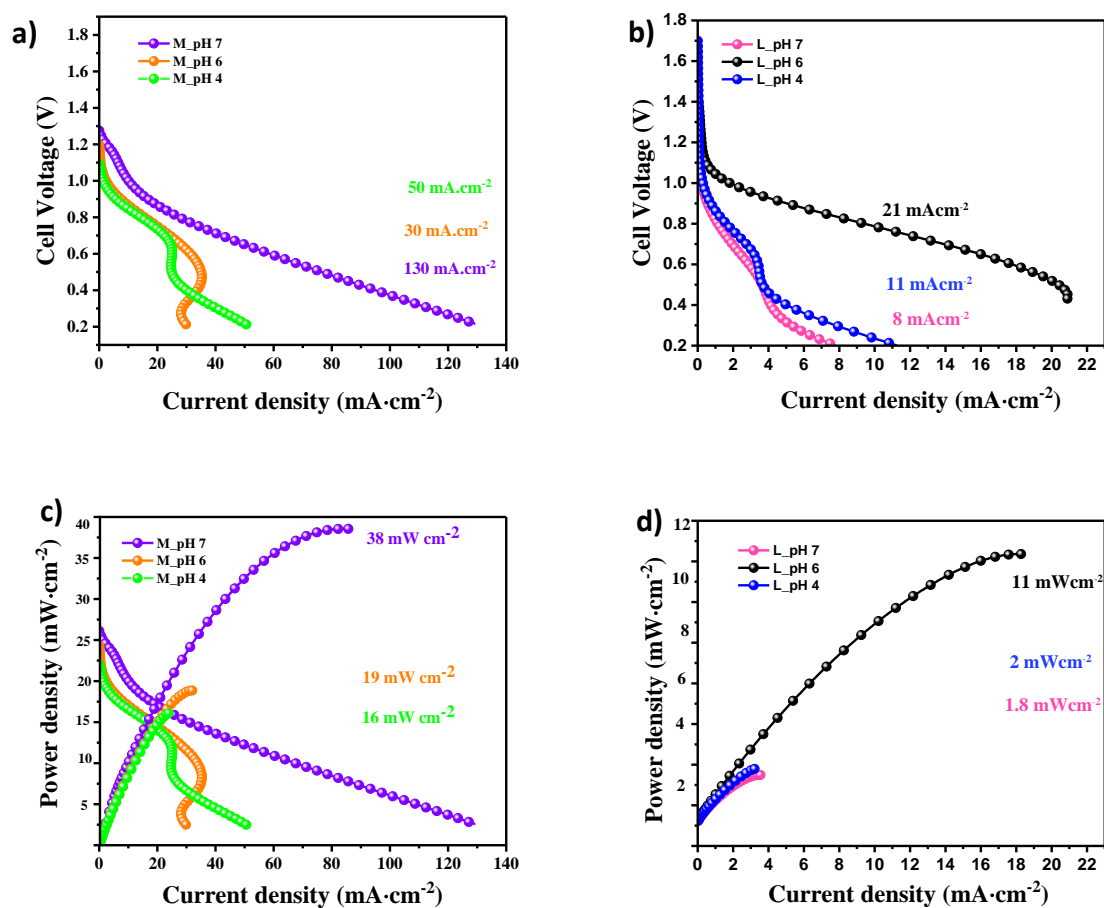
Figure 14. Polarization curves of electrolyte systems in the ZAB prototype. (a) and (c) GPE system. (b) and (d) Liquid system.

To analyse the discharge performance of the electrolytes, the galvanostatic discharge test was performed at a current density of 1.98 mA.cm^{-2} at room temperature. The GPE systems (Figure 15a), at pH 7 (M_pH 7), the battery delivered an exceptional specific capacity of 675 mAhg^{-1} over a substantial operational period of 8.66 hours. This result outperformed several reported hydrogel-based systems. For instance, the PAM–cellulose nanofiber hydrogel [142], at its best achieved 300 mAh.g^{-1} at 50 °C, and the acetamide/zinc perchlorate hexahydrate/PAM system [143] reached 250 mAh.g^{-1}. Furthermore, at pH 6 (M_pH 6), the specific capacity decreased to 342 mAh.g^{-1} with a shorter run time of 3.28 hours. This

suggested that the polymeric matrix may still facilitate efficient electrochemical reactions, although the lower pH appears to quicken the discharge process. However, this result surpasses the PAM/ZnSO$_4$/Glycerol/xanthan gum combination, which delivered 125 mAh·g^{-1} at 0 °C [144] and the PAM cross-linked with DMSO and cellulose nanofibers, which attained 118 mAh·g^{-1} at −20 °C [145]. Moreover, at pH 4 (M_pH 4), the specific capacity was reduced to 184 mAhg^{-1}, with the operational time dropping to 2.50 hours. The acidic conditions at this pH level are likely less conducive to the zinc-air battery's chemistry within the polymeric matrix, leading to diminished performance.

In the liquid electrolyte system using only a ZnCl$_2$+NH$_4$Cl solution (Figure 15a), at pH 7 (L_pH 7), the highest specific capacity of 724 mAh.g^{-1} is achieved, and the system maintains voltage for over 24 hours, demonstrating the capability of the liquid electrolyte to sustain prolonged discharge without the structural support of a polymer matrix. However, the post-Morten SEM images (presented in Appendices, Figure A3 and Figure A4) and EDS (Figure 18) data of the anode revealed significant zinc deposition and substantial degradation, characteristic of severe galvanic corrosion. These conditions are likely due to the uncontrolled mobility of ions in the liquid state, which, while enabling high discharge capacity, also intensifies zinc corrosion and deposition [75], [76]. Moreover, as the pH decreased to pH 6 (L_pH 6), there was a noticeable reduction in specific capacity to 418 mAh.g^{-1}, an operational time diminished to just 1.52 hours. This decline in performance may be attributed to a less favourable reaction kinetics due to the absence of a polymer matrix, compounded by the chemically aggressive environment that accelerates zinc corrosion as suggested by the Pourbaix diagram for zinc [73], [74]. Further reduction in pH to 4 (L_pH 4) exhibited the specific capacity stabilize near 410 mAh.g^{-1}, nonetheless operational time further decreased to 0.87 hours. Therefore, it can be stated that while the liquid electrolyte could maintain zinc reactivity, it did so at the cost of a significantly reduced lifespan due to the heightened corrosive conditions, which exacerbated the degradation and deposition on the zinc electrode, ultimately undermining the electrodes structural integrity and reducing its operational durability.
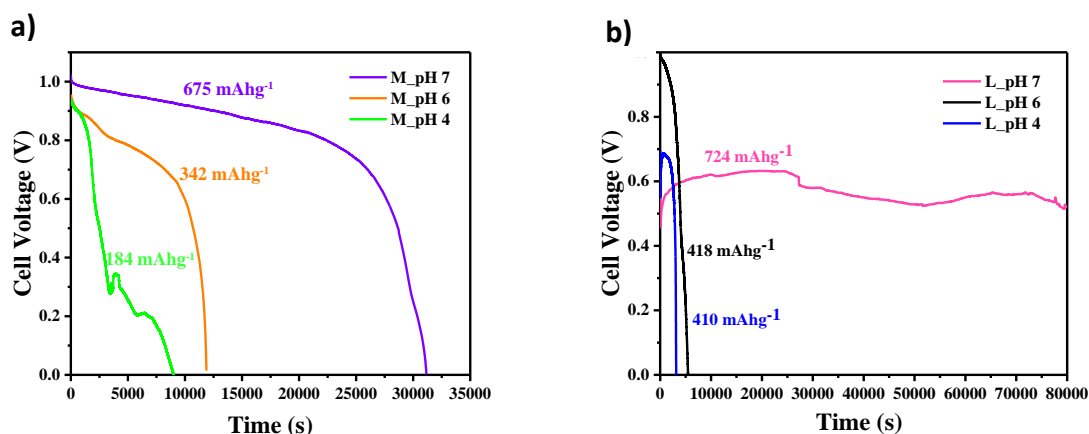
Figure 15. Discharge curves of the GPE and liquid electrolyte systems at a constant current of 1.98 mA.cm^{-1} in a ZAB prototype. (a) GPE system. (b) Liquid electrolyte system.

4.5. Post-Morten Physicochemical and Structural Characterization

4.5.1. FTIR analysis

The FTIR tests were conducted on all gel polymeric membranes after the discharge test, (Figure 16). The peaks around 3000-3500 cm^{-1} (O-H and N-H stretching vibrations) appeared to be sharper across all pH levels, which may indicate a restructuring of hydrogen bonds or an increase in residual water due to electrochemical reactions. Particularly at pH 6, the O-H stretching vibration was more intense, which could be due to the higher degree of hydration present in the electrolyte system. This could be related to the formation of specific zinc complexes that did not fully deplete the available water molecules for hydrogen bonding. At pH 7, the O-H signal is less pronounced, likely due to the formation of more stable zinc-ammine complexes that reduce the availability of free O-H groups. On the other hand, for GPE at pH 7, t at 2340 cm^{-1} may correspond to the asymmetric stretching vibration of carbon dioxide (CO_2) [113]. This was expected, as this GPE was exposed to the air for around 24 hours in total during the discharge battery test. The peak at 1550-1600 cm^{-1} can represent both the amide II band (N-H bending and C-N stretching) and potential contributions from C=O stretching. During the N-deacetylation of chitosan, the Amide I (C=O) and amide II (N-H) bands may overlap due to molecular interactions. According to [150], the amide I (C=O) band is typically observed at 1655 cm^{-1}, while the amide II (N-H) band appears around 1600 cm^{-1}, with possible overlap due to the interactions of the functional groups in chitosan. The peak's

intensity and sharpness are affected by the pH due to the protonation of nearby amine groups. Nevertheless, for the post-Morten spectra, there's an apparent shift or broadening in the post-discharge spectra, which could suggest changes in amide interactions, possibly due to complexation with zinc ions released during discharge. Furthermore, the peak near 1020-1080 cm^{-1} (C-O stretching vibrations), was expected to be consistent across different pH levels due to the stable polysaccharide structure.
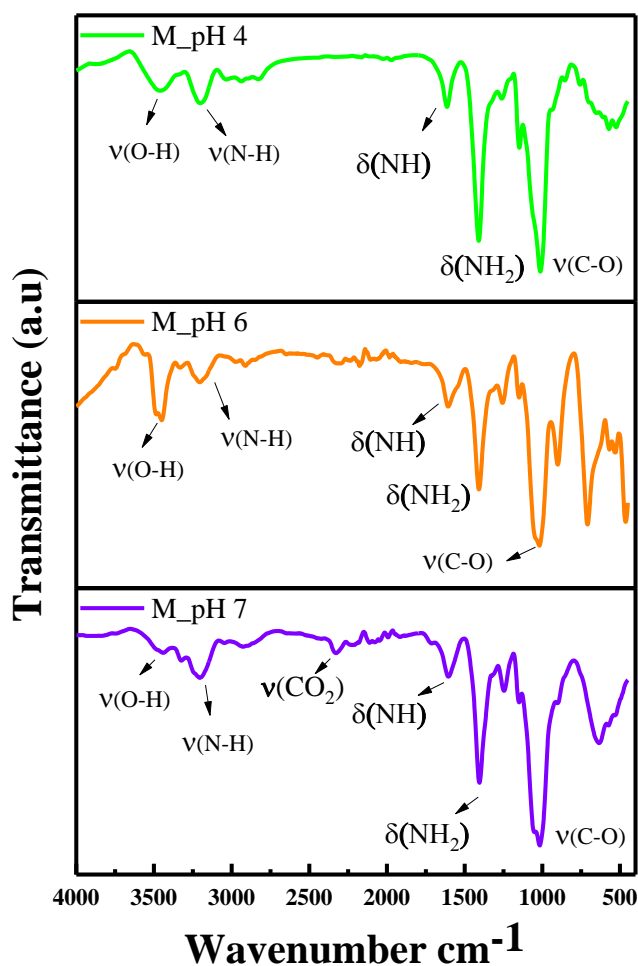

Figure 16. Post-Morten FTIR spectra of all GPEs.

4.5.2 Membrane post-mortem test SEM

The SEM images (Figure 17) revealed distinct differences in the microstructures of gel polymeric electrolytes, which can be attributed to the pH-dependent chemical interactions within the electrolyte, particularly affecting the formation and stability of zinc complexes.

At pH 4 (Figure 17, pH=4), the microstructure displayed a rough and heterogeneous surface with pronounced porosity and irregular features, suggesting a less stable gel matrix. This observation likely stems from the reduced complexation of Zn^{2+} ions with NH_3, as NH_3 is less available in acidic conditions. The harsh acidic environment may accelerate polymer degradation and disrupt zinc compound formations, leading to a more aggressive breakdown of the matrix structure. This aligns with findings from the literature that emphasize the critical role of pH in the solvation dynamics of zinc ions and their impact on the structural stability of battery electrolytes [151].

At pH 6 (Figure 17, pH=6) the transition to a more fibrous structure with visible formations of elongated, semi-crystalline deposits can be observed in (Figure 17, pH=6). This intermediate pH allowed for better availability of NH_3, enhancing more complex zinc-ammonia structures compared to the more acidic pH 4. The presence of intermediate complexes such as $Zn(NH_3)_3^{2+}$ seems to stabilize sections of the matrix, indicating significant interactions between the polymer and the electrolyte. Additionally, the dendrite formation observed at pH 6 can be attributed to the semi-stable nature of these zinc-ammonia complexes [126]. While these complexes provide some structural stability, their partial dissociation during the discharge process can release zinc ions that precipitate unevenly. This uneven deposition contributes to dendritic growth, which is problematic for battery safety and efficiency as it can lead to short circuits and uneven current distribution within the cell [152], [153].

On the other hand, the SEM images at pH 7 (Figure 17, pH=7), revealed the most uniform and cohesive structure among the tested conditions, characterized by decreased porosity and smoother areas. The high availability of NH_3 at this pH promotes the extensive formation of stable zinc-ammine complexes like $Zn(NH_3)_n^{2+}$, which contribute to a denser and more stable polymer network. This suggests enhanced structural integrity and potentially improved electrolyte performance due to more uniform ion transport pathways. The formation and stability of these complexes are critical for enhancing the performance and durability of zinc-based batteries as discussed in [50].
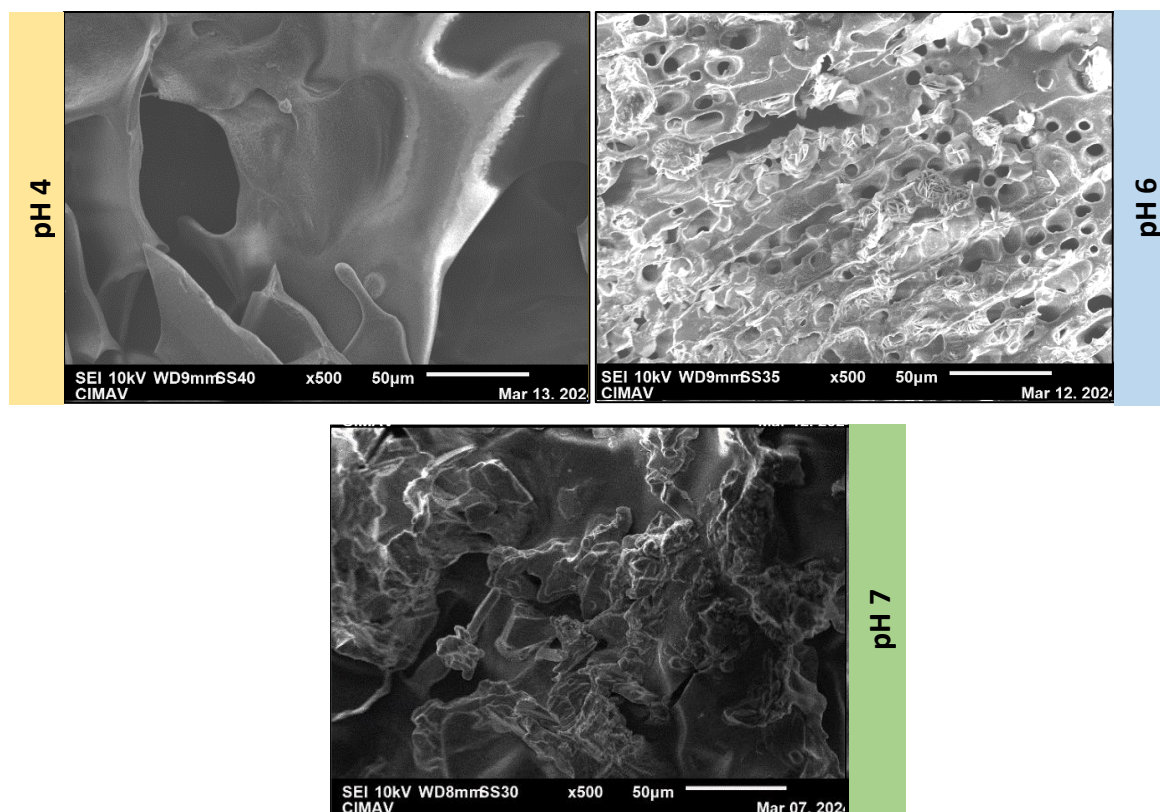
Figure 17. Micrographs of the gel polymeric system post-Mortem.

In addition to the SEM tests, EDS was used to determine the overall elemental composition of various electrolytes used in the study (Figure 18), focusing on the mass percentages of zinc (Zn) and chlorine (Cl) after discharge. The electrolyte conditions are labelled as follows: GPE at pH 7 (M_pH 7), GPE at pH 6 (M_pH 6), GPE cathode side at pH 6 (MC_pH 6), GPE anode side at pH 6 (MA_pH 6), liquid electrolyte anode side at pH 6 (LA_pH 6), and liquid electrolyte cathode side at pH 6 (LC_pH 6).

In this manner, by analysing the data provided from the EDS analysis, there is a notable difference in the chemical composition between the gel polymeric electrolyte systems, which can be linked to the dendritic structures observed in the post-Morten SEM images of GPEs at pH 4 and pH 6). The EDS for the M_pH6 sample showed more pronounced dendritic formations, the Zn content is significantly higher at 38.26% compared to 21.74% in the M_pH7. This indicates a higher concentration of zinc in areas where dendritic structures are forming. The increased presence of zinc correlates with the tendency to form dendritic structures due to the localized supersaturation of zinc ions which precipitate out as dendrites during the discharge process (also observed in the SEM micrographs from GPE anode and cathode side presented in the Appendices (Figure A1, Figure A2, Figure A3, and Figure A4).

Additionally, the elevated levels of chlorine in the dendrite-rich EDS data (M_pH7 with 25.15% compared to M_pH6 with 13.97%) support the idea that chlorine from the electrolyte is also incorporated into the dendrites, possibly influencing their growth dynamics and morphology. Moreover, the EDS of the liquid anode SEM (LA_pH7) shows a Zn content of 69.7%. Even though this condition exhibited a greater specific capacity (as mentioned in the Battery Evaluation Section), the severe zinc deposition severely compromised the electrolyte's integrity.
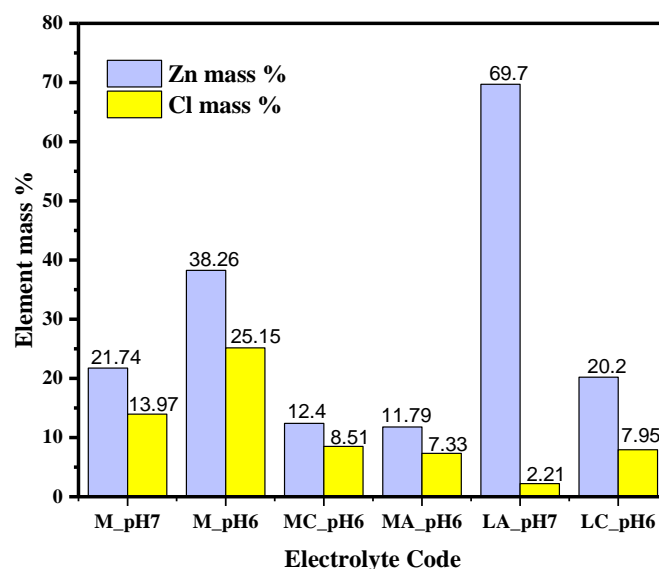

Figure 18. Elemental Composition of Electrolytes. The graph shows the mass percentages of Zinc (Zn) and Chlorine (Cl) in various electrolyte conditions after discharge at pH 6 and pH 7. Conditions include GPE system labels, cathode side, anode side, and liquid electrolyte system.

5. Conclusions

The comprehensive evaluation of chitosan-starch-based biopolymeric hydrogels embedded in near-neutral ionic solutions as electrolytes in zinc-air batteries has provided valuable insights into the electrochemical, structural, and functional behavior under varying pH conditions. Through methodical experimentation involving a range of analytical techniques, our study underlines the critical role of pH in optimizing battery performance, particularly emphasizing the benefits of near-neutral conditions.

- The GPEs were successfully synthesized and demonstrated effective performance as polymer matrices for near-neutral ionic solutions containing $ZnCl_2$ and NH_4Cl, with pH levels ranging from 4 to 7.

- FTIR analysis confirmed the successful cross-linking of chitosan and starch and revealed that higher pH levels improved ion transport and stability of the hydrogels, while acidic conditions at pH 4 decreased flexibility and porosity. The observed dehydration and hydrogen bond restructuring post-discharge highlighted the critical influence of pH on zinc ion interactions and electrochemical performance, essential for the optimization of ZABs.

- Thermogravimetric analysis (TGA) and scanning electron microscopy (SEM) results indicated that GPEs exhibited enhanced thermal stability and a more uniform microstructure at higher pH levels (6 and 7) due to the formation of stable zinc-ammine complexes. In contrast, acidic conditions led to a rougher surface texture and less stable water-polymer interactions.

- X-ray diffraction (XRD) confirmed the absence of unwanted solid precipitate products like Simonkolleite at pH 7, which supports efficient ion transport and the feasibility of ZABs reversibility.

- The electrochemical evaluation of GPEs in near-neutral ionic solutions demonstrated significantly improved performance, particularly at pH 7. The GPEs achieved notable power densities of 38 mW.cm^{-2} and specific capacities of 675 mAh.g^{-1}, outperforming traditional liquid electrolytes and established benchmarks. Furthermore, electrochemical impedance spectroscopy (EIS) and Cyclic voltammetry (CV) showed, reduced bulk resistances, increased ionic conductivities, and current density, as the

pH approached neutral values (pH 7), underscoring the potential of these GPEs to enhance the technology of ZABs.

6 Appendices

6.1 SEM micrographs anode and cathode side of GEPs and liquid electrolytes

6.1.1 Membrane Cathode Discharge SEM
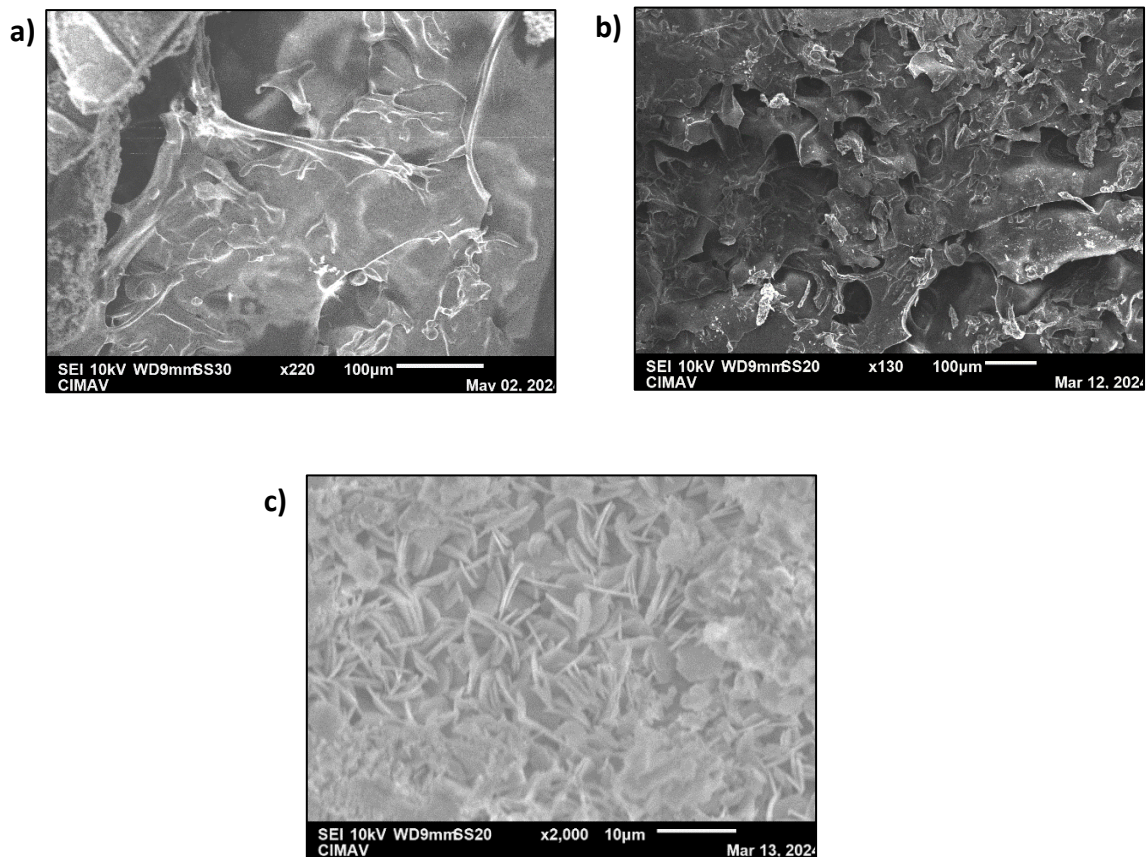
Figure A1. Post-Morten SEM micrographs of the cathode side at different pH values (a) pH_4 GPE, x2000 magnification. (b) pH_6 GPE, x100 magnification. (c) pH_7 GPE, x220 magnification.

6.1.2 Membrane Anode Discharge SEM

a)

b)
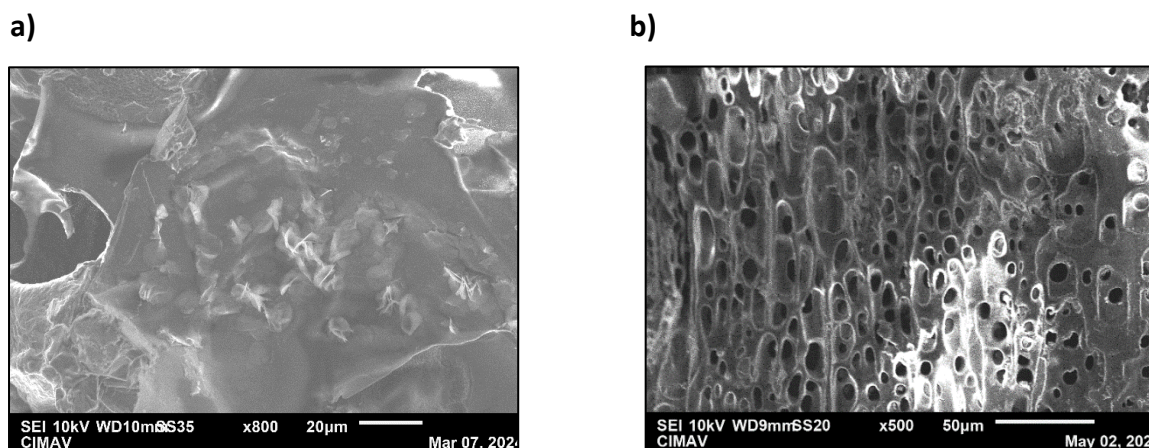
Figure A2. SEM micrographs of the cathode side at different pH values after discharge test. a) pH_7 GPE, x800 magnification. (b) pH_6 GPE, x500 magnification

6.1.3 Liquid Anode Discharge SEM

a)

b)

c)

Figure A3. Post-Morten SEM micrographs of the anode side of liquid electrolyte systems. (a) pH_7, x1000 magnification. (b) pH_6, x2000 magnification. (c) pH_4, x5000 magnification.

6.1.4 Liquid Cathode Discharge SEM
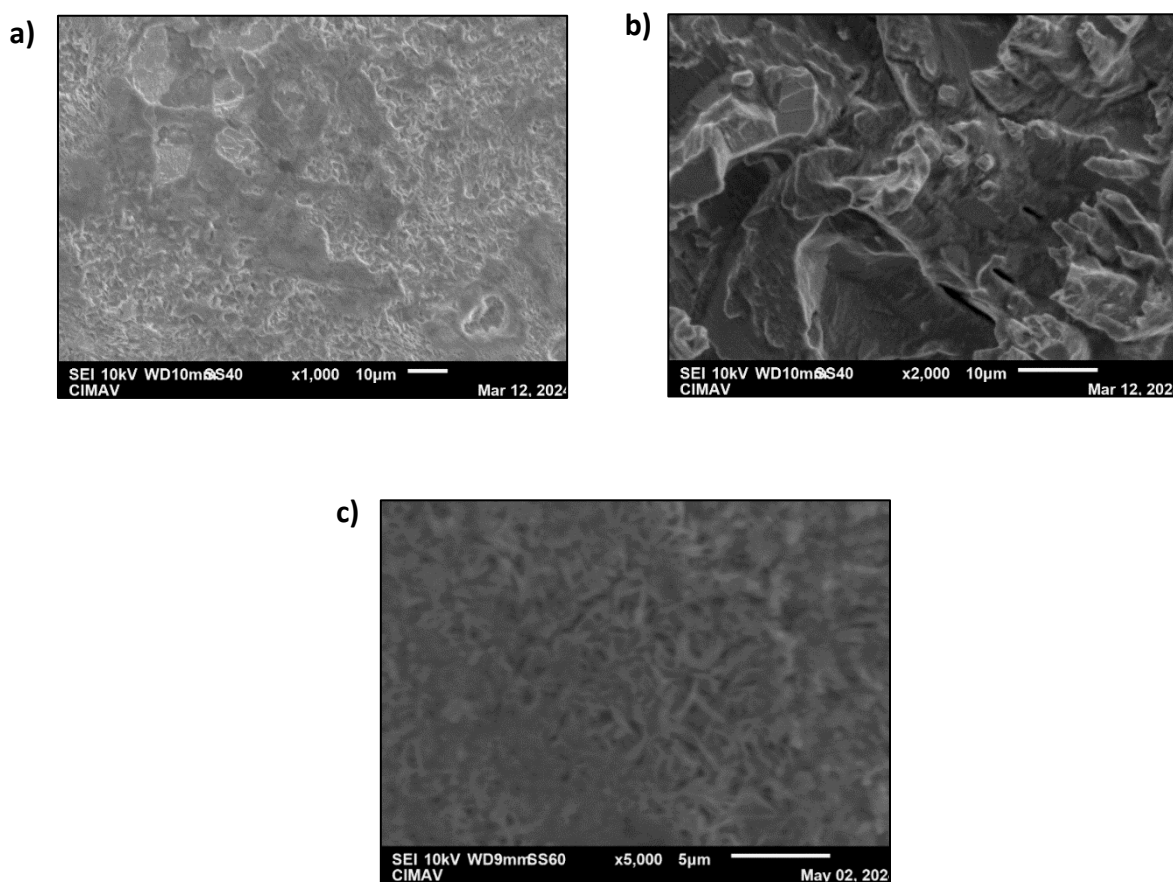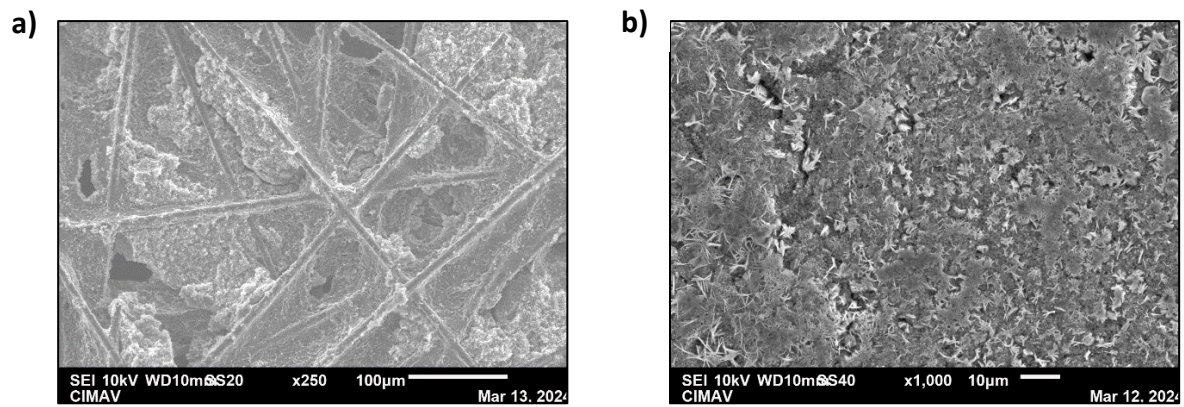
a)

b)

Figure A4. Post-Morten SEM micrographs of the liquid electrolyte's cathode side at different pH values. (a) pH_7, x1000 magnification. (b) pH_6, x1000 magnification.

References

[1] Prabhansu, *Emerging Trends in Energy Storage Systems and Industrial Applications* (Chap. 2, pp. 27-65). Elsevier, 2023. doi: 10.1016/C2020-0-03535-8.

[2] A. Jossen, "BATTERIES | Dynamics," in *Encyclopedia of Electrochemical Power Sources*, Elsevier, 2009, pp. 478–488. doi: 10.1016/B978-044452745-5.00940-0.

[3] M. Winter and R. J. Brodd, "What Are Batteries, Fuel Cells, and Supercapacitors?," *Chem Rev*, vol. 104, no. 10, pp. 4245–4270, Oct. 2004, doi: 10.1021/cr020730k.

[4] Y. Li and H. Dai, "Recent advances in zinc–air batteries," *Chem. Soc. Rev.*, vol. 43, no. 15, pp. 5257–5275, 2014, doi: 10.1039/C4CS00015C.

[5] G. Nazir *et al.*, "A Review of Rechargeable Zinc–Air Batteries: Recent Progress and Future Perspectives," *Nanomicro Lett*, vol. 16, no. 1, p. 138, Dec. 2024, doi: 10.1007/s40820-024-01328-1.

[6] J. Zhang, Z. Zhao, Z. Xia, and L. Dai, "A metal-free bifunctional electrocatalyst for oxygen reduction and oxygen evolution reactions," *Nat Nanotechnol*, vol. 10, no. 5, pp. 444–452, May 2015, doi: 10.1038/nnano.2015.48.

[7] K. Wu *et al.*, "Recent Advances in Polymer Electrolytes for Zinc Ion Batteries: Mechanisms, Properties, and Perspectives," *Adv Energy Mater*, vol. 10, no. 12, Mar. 2020, doi: 10.1002/aenm.201903977.

[8] Z. Pan *et al.*, "All-solid-state sponge-like squeezable zinc-air battery," *Energy Storage Mater*, vol. 23, pp. 375–382, Dec. 2019, doi: 10.1016/j.ensm.2019.04.036.

[9] J.-F. Drillet *et al.*, "Development of a Novel Zinc/Air Fuel Cell with a Zn Foam Anode, a PVA/KOH Membrane and a MnO$_2$/SiOC-Based Air Cathode," *ECS Trans*, vol. 28, no. 32, pp. 13–24, Oct. 2010, doi: 10.1149/1.3507923.

[10] H. Ma, C. Li, Y. Su, and J. Chen, "Studies on the vapour-transport synthesis and electrochemical properties of zinc micro-, meso- and nanoscale structures," *J. Mater. Chem.*, vol. 17, no. 7, pp. 684–691, 2007, doi: 10.1039/B609783A.

[11] Z. Guo, S. Zhao, T. Li, D. Su, S. Guo, and G. Wang, "Recent Advances in Rechargeable Magnesium-Based Batteries for High-Efficiency Energy Storage," *Adv Energy Mater*, vol. 10, no. 21, Jun. 2020, doi: 10.1002/aenm.201903591.

[12] P. Yao *et al.*, "Review on Polymer-Based Composite Electrolytes for Lithium Batteries," *Front Chem*, vol. 7, Aug. 2019, doi: 10.3389/fchem.2019.00522.

[13] Q. Zhao, S. Stalin, C.-Z. Zhao, and L. A. Archer, "Designing solid-state electrolytes for safe, energy-dense batteries," *Nat Rev Mater*, vol. 5, no. 3, pp. 229–252, Feb. 2020, doi: 10.1038/s41578-019-0165-5.

[14] J. Ming, J. Guo, C. Xia, W. Wang, and H. N. Alshareef, "Zinc-ion batteries: Materials, mechanisms, and applications," *Materials Science and Engineering: R: Reports*, vol. 135, pp. 58–84, Jan. 2019, doi: 10.1016/j.mser.2018.10.002.

[15] F. A. Getie, D. W. Ayele, N. G. Habtu, F. A. Yihun, and T. A. Yemata, "Development of electrolytes for rechargeable zinc-air batteries: current progress, challenges, and future outlooks," *SN Appl Sci*, vol. 4, no. 10, p. 270, Oct. 2022, doi: 10.1007/s42452-022-05156-z.

[16] M. H. Alfaruqi *et al.*, "Structural transformation and electrochemical study of layered MnO2 in rechargeable aqueous zinc-ion battery," *Electrochim Acta*, vol. 276, pp. 1–11, Jun. 2018, doi: 10.1016/j.electacta.2018.04.139.

[17] Elena Iriun, "Desarrollo de baterias secundarias de zinc-aire con electrolitos acuosos alternativos," Universidad de Barcelona, 2020.

[18] S. Lee, J. Choi, M. Kim, J. Park, M. Park, and J. Cho, "Material design and surface chemistry for advanced rechargeable zinc–air batteries," *Chem Sci*, vol. 13, no. 21, pp. 6159–6180, 2022, doi: 10.1039/D1SC07212A.

[19] F. Cheng and J. Chen, "Metal–air batteries: from oxygen reduction electrochemistry to cathode catalysts," *Chem Soc Rev*, vol. 41, no. 6, p. 2172, 2012, doi: 10.1039/c1cs15228a.

[20] C. You *et al.*, "Advances in rechargeable Mg batteries," *J Mater Chem A Mater*, vol. 8, no. 48, pp. 25601–25625, 2020, doi: 10.1039/D0TA09330K.

[21]   A. Iqbal, O. M. El-Kadri, and N. M. Hamdan, "Insights into rechargeable Zn-air batteries for future advancements in energy storing technology," *J Energy Storage*, vol. 62, p. 106926, Jun. 2023, doi: 10.1016/j.est.2023.106926.

[22]   J. Zhang, Q. Zhou, Y. Tang, L. Zhang, and Y. Li, "Zinc–air batteries: are they ready for prime time?," *Chem Sci*, vol. 10, no. 39, pp. 8924–8929, 2019, doi: 10.1039/C9SC04221K.

[23]   M. Park, J. Ryu, W. Wang, and J. Cho, "Material design and engineering of next-generation flow-battery technologies," *Nat Rev Mater*, vol. 2, no. 1, p. 16080, Nov. 2016, doi: 10.1038/natrevmats.2016.80.

[24]   J. Fu, Z. P. Cano, M. G. Park, A. Yu, M. Fowler, and Z. Chen, "Electrically Rechargeable Zinc–Air Batteries: Progress, Challenges, and Perspectives," *Advanced Materials*, vol. 29, no. 7, Feb. 2017, doi: 10.1002/adma.201604685.

[25]   Q. Wang, S. Kaushik, X. Xiao, and Q. Xu, "Sustainable zinc–air battery chemistry: advances, challenges and prospects," *Chem Soc Rev*, vol. 52, no. 17, pp. 6139–6190, 2023, doi: 10.1039/D2CS00684G.

[26]   J. Stamm, A. Varzi, A. Latz, and B. Horstmann, "Modeling nucleation and growth of zinc oxide during discharge of primary zinc-air batteries," *J Power Sources*, vol. 360, pp. 136–149, Aug. 2017, doi: 10.1016/j.jpowsour.2017.05.073.

[27]   J. Kuang, G. D. Renderos, K. J. Takeuchi, E. S. Takeuchi, A. C. Marschilok, and L. Wang, "Zinc–air batteries in neutral/near-neutral electrolytes," *Functional Materials Letters*, vol. 14, no. 07, Oct. 2021, doi: 10.1142/S1793604721300127.

[28]   C. Zhai *et al.*, "Electrolyte Additive Strategies for Suppression of Zinc Dendrites in Aqueous Zinc-Ion Batteries," *Batteries*, vol. 8, no. 10, p. 153, Oct. 2022, doi: 10.3390/batteries8100153.

[29]   K. Wang *et al.*, "Dendrite growth in the recharging process of zinc–air batteries," *J Mater Chem a Mater*, vol. 3, no. 45, pp. 22648–22655, 2015, doi: 10.1039/C5TA06366C.

[30] K. E. K. Sun *et al.*, "Suppression of Dendrite Formation and Corrosion on Zinc Anode of Secondary Aqueous Batteries," *ACS Appl Mater Interfaces*, vol. 9, no. 11, pp. 9681–9687, Mar. 2017, doi: 10.1021/acsami.6b16560.

[31] F. Moulai, T. Hadjersi, and A. Achour, "The effect of zinc shape on its corrosion mitigation as an anode in aqueous Zn/MnO_2 battery," *Journal of Electroanalytical Chemistry*, vol. 886, p. 115140, Apr. 2021, doi: 10.1016/j.jelechem.2021.115140.

[32] K. Xu, "Electrolytes and Interphases in Li-Ion Batteries and Beyond," *Chem Rev*, vol. 114, no. 23, pp. 11503–11618, Dec. 2014, doi: 10.1021/cr500003w.

[33] N. Zhang *et al.*, "Towards high-performance aqueous $Zn–MnO_2$ batteries: Formation mechanism and alleviation strategies of irreversible inert phases," *Compos B Eng*, vol. 260, p. 110770, Jul. 2023, doi: 10.1016/j.compositesb.2023.110770.

[34] Z. Xu, Q. Fan, Y. Li, J. Wang, and P. D. Lund, "Review of zinc dendrite formation in zinc bromine redox flow battery," *Renewable and Sustainable Energy Reviews*, vol. 127, p. 109838, Jul. 2020, doi: 10.1016/j.rser.2020.109838.

[35] "The Voltaic Battery," *Sci Am*, vol. 6, no. 1, pp. 3–3, Sep. 1850, doi: 10.1038/scientificamerican09211850-3.

[36] Georges lionel leclanche, "Electrical Battery with Primary and Secondary Piles Combined," 1867

[37] Takamura, T. (2019). Alkaline battery. In *Encyclopedia of electrochemical power sources* (Chap. 2, p. 271).

[38] L. W. J. Kuang, "Zinc-air batteries in neutral/near-neutral electrolytes," *Functional Materials Letters*, 2021. (Chap. 5, p. 174).

[39] J. B. Goodenough and Y. Kim, "Challenges for Rechargeable Li Batteries," *Chemistry of Materials*, vol. 22, no. 3, pp. 587–603, Feb. 2010, doi: 10.1021/cm901452z.

[40] A. López-Grande, G. C. Mather, and F. Muñoz, "Thermodynamic calculation of the ionic conductivity of LiPON glasses and solid electrolytes," *J Mater Chem a Mater*, vol. 11, no. 23, pp. 12282–12296, 2023, doi: 10.1039/D3TA00724C.

[41]   F. Zheng, M. Kotobuki, S. Song, M. O. Lai, and L. Lu, "Review on solid electrolytes for all-solid-state lithium-ion batteries," *J Power Sources*, vol. 389, pp. 198–213, Jun. 2018, doi: 10.1016/j.jpowsour.2018.04.022.

[42]   J. C. Bachman *et al.*, "Inorganic Solid-State Electrolytes for Lithium Batteries: Mechanisms and Properties Governing Ion Conduction," *Chem Rev*, vol. 116, no. 1, pp. 140–162, Jan. 2016, doi: 10.1021/acs.chemrev.5b00563.

[43]   R. Winand, *Modern Electroplating*, 5th ed. New Jersey: Hoboken. (Chap. 1, p. 75).

[44]   A. Sumboja *et al.*, "Durable rechargeable zinc-air batteries with neutral electrolyte and manganese oxide catalyst," *J Power Sources*, vol. 332, pp. 330–336, Nov. 2016, doi: 10.1016/j.jpowsour.2016.09.142.

[45]   J. L. Limpo and A. Luis, "Solubility of zinc chloride in ammoniacal ammonium chloride solutions," *Hydrometallurgy*, vol. 32, no. 2, pp. 247–260, Mar. 1993, doi: 10.1016/0304-386X(93)90028-C.

[46]   X. G. Zhang, *Corrosion and Electrochemistry of Zinc*. Boston, MA: Springer US, 1996. doi: 10.1007/978-1-4757-9877-7. (Chap. 3, p. 185).

[47]   R. Friess, "THE REACTIONS OF AMMONIA ON THE SYSTEM ZnCl 2 -NH 4 Cl-H 2 O," *J Am Chem Soc*, vol. 52, no. 8, pp. 3083–3087, Aug. 1930, doi: 10.1021/ja01371a007.

[48]   A. M. ; H. M. N. Bredland, "Mechanistic Insights in Quinone-Based Zinc Batteries with Nonaqueous Electrolytes," *J Electrochem Soc*, 2020. (Chap. 3, p. 51).

[49]   S. Zhao, H. An, and S. Chen, "A study of a high-power, ammonium chloride zinc/manganese dioxide dry battery," *J Power Sources*, vol. 76, no. 2, pp. 218–220, Dec. 1998, doi: 10.1016/S0378-7753(98)00155-4.

[50]   S. Clark, A. Latz, and B. Horstmann, "Rational Development of Neutral Aqueous Electrolytes for Zinc–Air Batteries," *ChemSusChem*, vol. 10, no. 23, pp. 4735–4747, Dec. 2017, doi: 10.1002/cssc.201701468.

[51]   C. Han, W. Li, H. K. Liu, S. Dou, and J. Wang, "Principals and strategies for constructing a highly reversible zinc metal anode in aqueous batteries," *Nano Energy*, vol. 74, p. 104880, Aug. 2020, doi: 10.1016/j.nanoen.2020.104880.

[52] N. H. , et al Khalid, "ZnCl$_2$- and NH$_4$Cl-hydroponics gel electrolytes for zinc–carbon batteries," *J Power Sources*, 2007, doi: 10.1016/j.jpowsour.2007.10.048. (Chap. 1, p. 7-28).

[53] T. B. R. David Linden, *Handbook of batteries*. 2001. (Chap. 2, p. 15-35).

[54] D. E. Fenton, J. M. Parker, and P. V. Wright, "Complexes of alkali metal ions with poly(ethylene oxide)," *Polymer (Guildf)*, vol. 14, no. 11, p. 589, Nov. 1973, doi: 10.1016/0032-3861(73)90146-8.

[55] A. Manuel Stephan, "Review on gel polymer electrolytes for lithium batteries," *Eur Polym J*, vol. 42, no. 1, pp. 21–42, Jan. 2006, doi: 10.1016/j.eurpolymj.2005.09.017.

[56] D. F. Shriver, "Polymer electrolytes I: General principles," in *Solid State Electrochemistry*, Cambridge University Press, 1994, pp. 95–118. doi: 10.1017/CBO9780511524790.006.

[57] P. G. Bruce, Ed., *Solid State Electrochemistry*. Cambridge University Press, 1994. doi: 10.1017/CBO9780511524790. (Chap. 4, p. 18-36).

[58] K. Kim, W. Chae, J. Kim, C. Kim, and T. Earmme, "Gel Polymer Electrolytes for Lithium-Ion Batteries Enabled by Photo Crosslinked Polymer Network," *Gels*, vol. 9, no. 12, p. 975, Dec. 2023, doi: 10.3390/gels9120975.

[59] Z. Liu, S. Zein El Abedin, and F. Endres, "Electrodeposition and stripping of zinc from an ionic liquid polymer gel electrolyte for rechargeable zinc-based batteries," *Journal of Solid State Electrochemistry*, vol. 18, no. 10, pp. 2683–2691, Oct. 2014, doi: 10.1007/s10008-014-2526-8.

[60] F. A. Getie, D. W. Ayele, N. G. Habtu, F. A. Yihun, and T. A. Yemata, "Development of electrolytes for rechargeable zinc-air batteries: current progress, challenges, and future outlooks," *SN Appl Sci*, vol. 4, no. 10, p. 270, Oct. 2022, doi: 10.1007/s42452-022-05156-z.

[61] S. Lorca, F. Santos, and A. J. Fernández Romero, "A Review of the Use of GPEs in Zinc-Based Batteries. A Step Closer to Wearable Electronic Gadgets and Smart Textiles," *Polymers (Basel)*, vol. 12, no. 12, p. 2812, Nov. 2020, doi: 10.3390/polym12122812.

[62] K. S. Ngai, S. Ramesh, K. Ramesh, and J. C. Juan, "A review of polymer electrolytes: fundamental, approaches and applications," *Ionics (Kiel)*, vol. 22, no. 8, pp. 1259–1279, Aug. 2016, doi: 10.1007/s11581-016-1756-4.

[63] M. Aslam, M. A. Kalyar, and Z. A. Raza, "Polyvinyl alcohol: A review of research status and use of polyvinyl alcohol based nanocomposites," *Polym Eng Sci*, vol. 58, no. 12, pp. 2119–2132, Dec. 2018, doi: 10.1002/pen.24855.

[64] Z. Cao, H. Hu, M. Wu, K. Tang, and T. Jiang, "Planar all-solid-state rechargeable Zn–air batteries for compact wearable energy storage," *J Mater Chem A Mater*, vol. 7, no. 29, pp. 17581–17593, 2019, doi: 10.1039/C9TA04569D.

[65] R. Zhang, N. Hashemi, M. Ashuri, and R. Montazami, "Advanced Gel Polymer Electrolyte for Lithium-Ion Polymer Batteries," in *ASME 2013 7th International Conference on Energy Sustainability*, American Society of Mechanical Engineers, Jul. 2013. doi: 10.1115/ES2013-18386.

[66] D. Lee, Y. H. Song, U. H. Choi, and J. Kim, "Highly Flexible and Stable Solid-State Supercapacitors Based on a Homogeneous Thin Ion Gel Polymer Electrolyte Using a Poly(dimethylsiloxane) Stamp," *ACS Appl Mater Interfaces*, vol. 11, no. 45, pp. 42221–42232, Nov. 2019, doi: 10.1021/acsami.9b14990.

[67] A. Manuel Stephan, "Review on gel polymer electrolytes for lithium batteries," *Eur Polym J*, vol. 42, no. 1, pp. 21–42, Jan. 2006, doi: 10.1016/j.eurpolymj.2005.09.017.

[68] S. Ramesh and L. C. Wen, "Investigation on the effects of addition of SiO2 nanoparticles on ionic conductivity, FTIR, and thermal properties of nanocomposite PMMA–LiCF3SO3–SiO2," *Ionics (Kiel)*, vol. 16, no. 3, pp. 255–262, Apr. 2010, doi: 10.1007/s11581-009-0388-3.

[69] A. Manuel Stephan, "Review on gel polymer electrolytes for lithium batteries," *Eur Polym J*, vol. 42, no. 1, pp. 21–42, Jan. 2006, doi: 10.1016/j.eurpolymj.2005.09.017.

[70] F. Croce, G. B. Appetecchi, L. Persi, and B. Scrosati, "Nanocomposite polymer electrolytes for lithium batteries," *Nature*, vol. 394, no. 6692, pp. 456–458, Jul. 1998, doi: 10.1038/28818.

[71]   K. S. Ngai, S. Ramesh, K. Ramesh, and J. C. Juan, "A review of polymer electrolytes: fundamental, approaches and applications," *Ionics (Kiel)*, vol. 22, no. 8, pp. 1259–1279, Aug. 2016, doi: 10.1007/s11581-016-1756-4.

[72]   M. Aslam, M. A. Kalyar, and Z. A. Raza, "Polyvinyl alcohol: A review of research status and use of polyvinyl alcohol based nanocomposites," *Polym Eng Sci*, vol. 58, no. 12, pp. 2119–2132, Dec. 2018, doi: 10.1002/pen.24855.

[73]   J. Ding *et al.*, "Recent Advances in Biopolymer-Based Hydrogel Electrolytes for Flexible Supercapacitors," *ACS Energy Lett*, vol. 9, no. 4, pp. 1803–1825, Apr. 2024, doi: 10.1021/acsenergylett.3c02567.

[74]   K. Wu *et al.*, "Recent Advances in Polymer Electrolytes for Zinc Ion Batteries: Mechanisms, Properties, and Perspectives," *Adv Energy Mater*, vol. 10, no. 12, Mar. 2020, doi: 10.1002/aenm.201903977.

[75]   S. Peter, N. Lyczko, D. Gopakumar, H. J. Maria, A. Nzihou, and S. Thomas, "Chitin and Chitosan Based Composites for Energy and Environmental Applications: A Review," *Waste Biomass Valorization*, vol. 12, no. 9, pp. 4777–4804, Sep. 2021, doi: 10.1007/s12649-020-01244-6.

[76]   F. Hong *et al.*, "Chitosan-based hydrogels: From preparation to applications, a review," *Food Chem X*, vol. 21, p. 101095, Mar. 2024, doi: 10.1016/j.fochx.2023.101095.

[77]   C. Ma *et al.*, "All-Starch-Based Hydrogel for Flexible Electronics: Strain-Sensitive Batteries and Self-Powered Sensors," *ACS Sustain Chem Eng*, vol. 10, no. 20, pp. 6724–6735, May 2022, doi: 10.1021/acssuschemeng.2c00872.

[78]   M. F. Bósquez-Cáceres, J. Bejar, L. Álvarez-Contreras, and J. P. Tafur, "Enhancing Electrochemical Performance of Zinc-Air Batteries Using Freeze Crosslinked Carboxymethylcellulose-Chitosan Hydrogels as Electrolytes," *J Electrochem Soc*, vol. 170, no. 6, p. 060502, Jun. 2023, doi: 10.1149/1945-7111/acd876.

[79]   M. F. Bósquez-Cáceres *et al.*, "Chitosan-Carboxymethylcellulose Hydrogels as Electrolytes for Zinc–Air Batteries: An Approach to the Transition towards Renewable Energy Storage Devices," *Batteries*, vol. 8, no. 12, p. 265, Nov. 2022, doi: 10.3390/batteries8120265.

[80] Y. Yan *et al.*, "Tough Hydrogel Electrolytes for Anti-Freezing Zinc-Ion Batteries," *Advanced Materials*, vol. 35, no. 18, May 2023, doi: 10.1002/adma.202211673.

[81] S. Taokaew, "Recent Advances in Cellulose-Based Hydrogels Prepared by Ionic Liquid-Based Processes," *Gels*, vol. 9, no. 7, p. 546, Jul. 2023, doi: 10.3390/gels9070546.

[82] L. Díaz-Patiño *et al.*, "Zinc-Air Battery Operated with Modified-Zinc Electrodes/Gel Polymer Electrolytes," *ChemElectroChem*, vol. 9, no. 12, Jun. 2022, doi: 10.1002/celc.202200222.

[83] S. et al. Clark, "Towards Rechargeable Zinc-Air Batteries with Aqueous Chloride Electrolytes," *J. Electrochem. Soc*, doi: https://doi.org/10.1039/C9TA01190K. (Chap. 2, p. 271).

[84] R. M. Smith and A. E. Martell, *Critical Stability Constants," Inorganic Complexes*, vol. 4. New York and London: Plenum Press, 1976. (Chap. 1, p. 63-68).

[85] A. R. Mainar *et al.*, "An overview of progress in electrolytes for secondary zinc-air batteries and other storage systems based on zinc," *J Energy Storage*, vol. 15, pp. 304–328, Feb. 2018, doi: 10.1016/j.est.2017.12.004.

[86] C.-Y. Lai, Y.-T. Lu, W.-Y. Jao, H.-Y. Chen, and C.-C. Hu, "Near-neutral flexible zinc-air batteries with high power densities and long cycle life using chloride-based gel polymer electrolytes," *Electrochem commun*, vol. 136, p. 107240, Mar. 2022, doi: 10.1016/j.elecom.2022.107240.

[87] J. Jindra, J. Mrha, and M. Musilov, "Zinc-air cell with neutral electrolyte," *J Appl Electrochem*, vol. 3, no. 4, pp. 297–301, Nov. 1973, doi: 10.1007/BF00613036.

[88] S. Clark *et al.*, "Designing Aqueous Organic Electrolytes for Zinc–Air Batteries: Method, Simulation, and Validation," *Adv Energy Mater*, vol. 10, no. 10, Mar. 2020, doi: 10.1002/aenm.201903470. (Chap. 3, p. 86-89).

[89] G. Leclanché, "Quelques observations sur l'emploi des piles électriques. Pile constante au peroxyde de manganèse à un seul liquide," 1867.

[90] G. Jenson, G. Singh, J. K. Bhama, and A. Ratner, "Hydrogel Leclanché Cell: Construction and Characterization," *Energies (Basel)*, vol. 13, no. 3, p. 594, Jan. 2020, doi: 10.3390/en13030594.

[91] F. Trinidad, M. C. Montemayor, and E. Fatás, "Performance Study of $Zn / ZnCl_2$, NH_4Cl / Polyaniline / Carbon Battery," *J Electrochem Soc*, vol. 138, no. 11, pp. 3186–3189, Nov. 1991, doi: 10.1149/1.2085390.

[92] W. He *et al.*, "Challenges and strategies of zinc anode for aqueous zinc-ion batteries," *Mater Chem Front*, vol. 5, no. 5, pp. 2201–2217, 2021, doi: 10.1039/D0QM00693A.

[93] Q. Pan, D. Gong, and Y. Tang, "Recent progress and perspective on electrolytes for sodium/potassium-based devices," *Energy Storage Mater*, vol. 31, pp. 328–343, Oct. 2020, doi: 10.1016/j.ensm.2020.06.025.

[94] D. T. Hallinan, I. Villaluenga, and N. P. Balsara, "Polymer and composite electrolytes," *MRS Bull*, vol. 43, no. 10, pp. 759–767, Oct. 2018, doi: 10.1557/mrs.2018.212.

[95] J. Mindemark, M. J. Lacey, T. Bowden, and D. Brandell, "Beyond PEO—Alternative host materials for Li^+ -conducting solid polymer electrolytes," *Prog Polym Sci*, vol. 81, pp. 114–143, Jun. 2018, doi: 10.1016/j.progpolymsci.2017.12.004.

[96] G. Rollo-Walker, N. Malic, X. Wang, J. Chiefari, and M. Forsyth, "Development and Progression of Polymer Electrolytes for Batteries: Influence of Structure and Chemistry," *Polymers (Basel)*, vol. 13, no. 23, p. 4127, Nov. 2021, doi: 10.3390/polym13234127.

[97] A. Virya and K. Lian, "A review of neutral pH polymer electrolytes for electrochemical capacitors: Transitioning from liquid to solid devices," *Materials Reports: Energy*, vol. 1, no. 1, p. 100005, Feb. 2021, doi: 10.1016/j.matre.2020.12.002.

[98] Z. Li *et al.*, "Ionic Conduction in Polymer-Based Solid Electrolytes," *Advanced Science*, vol. 10, no. 10, Apr. 2023, doi: 10.1002/advs.202201718.

[99] B. A. Abdulkadir *et al.*, "Optimization of the Electrochemical Performance of a Composite Polymer Electrolyte Based on PVA-K_2CO_3-SiO_2 Composite," *Polymers*

(Basel), vol. 13, no. 1, p. 92, Dec. 2020, doi: 10.3390/polym13010092. (Chap. 4, p. 152-157).

[100] M. Tawalbeh, A. Al-Othman, A. Ka'ki, S. Mohamad, and M. Faheem Hassan, "Starch-chitosan-ionic liquids-based composite membranes for high temperature PEM fuel cells applications," *Int J Hydrogen Energy*, Jan. 2024, doi: 10.1016/j.ijhydene.2023.12.161.

[101] Thrisha K and Saratha R, "Natural polymer-based electrolytes for energy storage devices—an overview," *Ionics (Kiel)*, vol. 30, no. 3, pp. 1245–1266, Mar. 2024, doi: 10.1007/s11581-023-05315-1.

[102] M. I. Cruz-Balaz, M. F. Bósquez-Cáceres, J. Béjar, L. Álvarez-Contreras, V. M. Córdova, and J. P. Tafur, "Synthesis and characterization of Chitosan-Avocado seed starch hydrogels as electrolytes for zinc-air batteries," *Journal of Polymer Research*, vol. 30, no. 6, p. 189, Jun. 2023, doi: 10.1007/s10965-023-03566-0.

[103] M. F. Bósquez-Cáceres *et al.*, "Chitosan-Carboxymethylcellulose Hydrogels as Electrolytes for Zinc–Air Batteries: An Approach to the Transition towards Renewable Energy Storage Devices," *Batteries*, vol. 8, no. 12, p. 265, Nov. 2022, doi: 10.3390/batteries8120265.

[104] Elena Iruin Amatriain, "Desarrollo de Baterias Secundarias de Zinc Aire con electrolitos acuosos alternativos," Universidad de Barcelona, Barcelona, 2020.

[105] F. W. Thomas Goh *et al.*, "A Near-Neutral Chloride Electrolyte for Electrically Rechargeable Zinc-Air Batteries," *J Electrochem Soc*, vol. 161, no. 14, pp. A2080–A2086, Oct. 2014, doi: 10.1149/2.0311414jes.

[106] S. Clark, A. Latz, and B. Horstmann, "Rational Development of Neutral Aqueous Electrolytes for Zinc–Air Batteries," *ChemSusChem*, vol. 10, no. 23, pp. 4735–4747, Dec. 2017, doi: 10.1002/cssc.201701468.

[107] H. ; B. K. . Putz, "Match! -Phase Analysis Using Powder Diffraction."

[108] María I. Cruz-Balaz, et al, "Synthesis and characterization of Chitosan-Avocado seed starch hydrogels as electrolytes for zinc-air batteries," *Journal of Polymer Research*, 2023.

[109] L. Díaz-Patiño *et al.*, "Zinc-Air Battery Operated with Modified-Zinc Electrodes/Gel Polymer Electrolytes," *ChemElectroChem*, vol. 9, no. 12, Jun. 2022, doi: 10.1002/celc.202200222.

[110] T. Dai, M. Tanaka, Y.-Y. Huang, and M. R. Hamblin, "Chitosan preparations for wounds and burns: antimicrobial and wound-healing effects," *Expert Rev Anti Infect Ther*, vol. 9, no. 7, pp. 857–879, Jul. 2011, doi: 10.1586/eri.11.59.

[111] G. Kyzas and D. Bikiaris, "Recent Modifications of Chitosan for Adsorption Applications: A Critical and Systematic Review," *Mar Drugs*, vol. 13, no. 1, pp. 312–337, Jan. 2015, doi: 10.3390/md13010312.

[112] J. Fu, F. Yang, and Z. Guo, "The chitosan hydrogels: from structure to function," *New Journal of Chemistry*, vol. 42, no. 21, pp. 17162–17180, 2018, doi: 10.1039/C8NJ03482F.

[113] George Socrates, *Infrared and Raman Characteristic Group Frequencies: Tables and Charts*, 3rd Edition. 2011.

[114] Brian C. Smith, *Fundamentals of Fourier Transform Infrared Spectroscopy*, 11th ed. CRC Press, 2011.

[115] S. Majumdar and R. Ray, "Ionic conduction and charge carrier relaxation in chitosan acetate based solid biopolymer electrolyte embedded with LiClO4," *Journal of Polymer Research*, vol. 28, no. 5, p. 157, May 2021, doi: 10.1007/s10965-021-02509-x.

[116] E. Guibal, "Interactions of metal ions with chitosan-based sorbents: a review," *Sep Purif Technol*, vol. 38, no. 1, pp. 43–74, Jul. 2004, doi: 10.1016/j.seppur.2003.10.004.

[117] A. Pestov and S. Bratskaya, "Chitosan and Its Derivatives as Highly Efficient Polymer Ligands," *Molecules*, vol. 21, no. 3, p. 330, Mar. 2016, doi: 10.3390/molecules21030330. (Chap. 4, p. 56-75).

[118] R. A. A. Muzzarelli and C. Muzzarelli, "Chitosan Chemistry: Relevance to the Biomedical Sciences," in *Polysaccharides I*, Berlin/Heidelberg: Springer-Verlag, pp. 151–209. doi: 10.1007/b136820.

[119] L. W. Jerry Workman, *Infrared Spectroscopy of Organic Compounds*. 2000.

[120] Z. E. Rojudi *et al.*, "Effect of ethylene carbonate addition on ion aggregates, ion pairs and free ions of polyvinyl alcohol-methylcellulose host: Selection of polymer electrolyte for possible energy devices application," *Journal of Polymer Research*, vol. 29, no. 6, p. 248, Jun. 2022, doi: 10.1007/s10965-022-03098-z.

[121] H. Xu and S. Matysiak, "Effect of pH on chitosan hydrogel polymer network structure," *Chemical Communications*, vol. 53, no. 53, pp. 7373–7376, 2017, doi: 10.1039/c7cc01826f. (Accessed April 15, 2024).

[122] B. Cheng, B. Pei, Z. Wang, and Q. Hu, "Advances in chitosan-based superabsorbent hydrogels," *RSC Adv*, vol. 7, no. 67, pp. 42036–42046, 2017, doi: 10.1039/C7RA07104C.

[123] D. N. Iqbal *et al.*, "Nanocellulose/wood ash-reinforced starch–chitosan hydrogel composites for soil conditioning and their impact on pea plant growth," *RSC Adv*, vol. 14, no. 13, pp. 8652–8664, 2024, doi: 10.1039/D3RA08725E.

[124] G. Tesoro, "Textbook of polymer science, 3rd ed., Fred W. Billmeyer, Jr., Wiley-Interscience, New York, 1984, 578 pp. No price given.," *Journal of Polymer Science: Polymer Letters Edition*, vol. 22, no. 12, pp. 674–674, Dec. 1984, doi: 10.1002/pol.1984.130221210.

[125] K. Encalada, et al, "An overview of starch-based biopolymers and their biodegradability," 2018, [Online]. Available: http://www.redalyc.org/articulo.oa?id=507557607005

[126] F. W. Thomas Goh *et al.*, "A Near-Neutral Chloride Electrolyte for Electrically Rechargeable Zinc-Air Batteries," *J Electrochem Soc*, vol. 161, no. 14, pp. A2080–A2086, Oct. 2014, doi: 10.1149/2.0311414jes.

[127] M. I. Cruz-Balaz *et al.*, "Green Energy Storage: Chitosan-Avocado Starch Hydrogels for a Novel Generation of Zinc Battery Electrolytes," *Polymers (Basel)*, vol. 15, no. 22, p. 4398, Nov. 2023, doi: 10.3390/polym15224398.

[128] Y. Ma, et al , "Ionic conductivity enhancement in gel polymer electrolyte membrane with N-methyl-N-butyl-piperidine-bis(trifluoromethylsulfonyl) imide ionic liquid for lithium ion battery," *Colloids Surf A Physicochem Eng Asp*, vol. 502, pp. 130–138, Aug. 2016, doi: 10.1016/j.colsurfa.2016.05.011.

[129] F. Hu, et al, "The Gel-State Electrolytes in Zinc-Ion Batteries," *Batteries*, vol. 8, no. 11, p. 214, Nov. 2022, doi: 10.3390/batteries8110214.

[130] S. B. Aziz *et al.*, "An Investigation into the PVA:MC:NH4Cl-Based Proton-Conducting Polymer-Blend Electrolytes for Electrochemical Double Layer Capacitor (EDLC) Device Application: The FTIR, Circuit Design and Electrochemical Studies," *Molecules*, vol. 27, no. 3, p. 1011, Feb. 2022, doi: 10.3390/molecules27031011.

[131] J. S, "AC Impedance and FTIR Studies of PVA-ZnCl2 Based Solid Polymer Electrolytes," *Organic Polymer Material Research*, vol. 3, no. 1, pp. 1–4, Oct. 2021, doi: 10.30564/opmr.v3i1.3561.

[132] C. Wang, X. Zeng, P. J. Cullen, and Z. Pei, "The rise of flexible zinc-ion hybrid capacitors: advances, challenges, and outlooks," *J Mater Chem A Mater*, vol. 9, no. 35, pp. 19054–19082, 2021, doi: 10.1039/D1TA02775A.

[133] L. Yu *et al.*, "Recent progress on carbon materials for emerging zinc-ion hybrid capacitors," *J Mater Chem A Mater*, vol. 12, no. 16, pp. 9400–9420, 2024, doi: 10.1039/D4TA00252K.

[134] Y. Wang, et al , "Status and Opportunities of Zinc Ion Hybrid Capacitors: Focus on Carbon Materials, Current Collectors, and Separators," *Nanomicro Lett*, vol. 15, no. 1, p. 78, Dec. 2023, doi: 10.1007/s40820-023-01065-x.

[135] C. Y. Lai, et al, "Near-neutral flexible zinc-air batteries with high power densities and long cycle life using chloride-based gel polymer electrolytes," *Electrochem commun*, vol. 136, Mar. 2022, doi: 10.1016/j.elecom.2022.107240.

[136]   C. Lin *et al.*, "Solid-State Rechargeable Zinc–Air Battery with Long Shelf Life Based on Nanoengineered Polymer Electrolyte," *ChemSusChem*, vol. 11, no. 18, pp. 3215–3224, Sep. 2018, doi: 10.1002/cssc.201801274.

[137]   Y. Li *et al.*, "Long-battery-life flexible zinc-air battery with near-neutral polymer electrolyte and nanoporous integrated air electrode," *J Mater Chem A Mater*, vol. 7, no. 44, pp. 25449–25457, 2019, doi: 10.1039/c9ta09137h.

[138]   S. Hosseini, S. Masoudi Soltani, and Y.-Y. Li, "Current status and technical challenges of electrolytes in zinc–air batteries: An in-depth review," *Chemical Engineering Journal*, vol. 408, p. 127241, Mar. 2021, doi: 10.1016/j.cej.2020.127241.

[139]   Y. Geng *et al.*, "Electrolyte additive engineering for aqueous Zn ion batteries," *Energy Storage Mater*, vol. 51, pp. 733–755, Oct. 2022, doi: 10.1016/j.ensm.2022.07.017.

[140]   D. Ji and J. Kim, "Trend of Developing Aqueous Liquid and Gel Electrolytes for Sustainable, Safe, and High-Performance Li-Ion Batteries," Dec. 01, 2024, *Springer Science and Business Media B.V.* doi: 10.1007/s40820-023-01220-4.

[141]   M. D. Tikekar, S. Choudhury, Z. Tu, and L. A. Archer, "Design principles for electrolytes and interfaces for stable lithium-metal batteries," *Nat Energy*, vol. 1, no. 9, p. 16114, Sep. 2016, doi: 10.1038/nenergy.2016.114.

[142]   W. et al. Xu, "A stretchable solid-state zinc ion battery based on a cellulose nanofiber–polyacrylamide hydrogel electrolyte and a Mg0.23V2O5 ·1.0H2O cathode," *J Mater Chem*, pp. 18327–18337, 2020, doi: https://doi.org/10.1039/D0TA06467J.

[143]   J. Huang, X. Chi, Y. Du, Q. Qiu, and Y. Liu, "Ultrastable Zinc Anodes Enabled by Anti-Dehydration Ionic Liquid Polymer Electrolyte for Aqueous Zn Batteries," *ACS Appl Mater Interfaces*, vol. 13, no. 3, pp. 4008–4016, Jan. 2021, doi: 10.1021/acsami.0c20241.

[144]   Y. Deng, Y. Wu, L. Wang, K. Zhang, Y. Wang, and L. Yan, "Polysaccharide hydrogel electrolytes with robust interfacial contact to electrodes for quasi-solid state flexible aqueous zinc ion batteries with efficient suppressing of dendrite growth," *J Colloid Interface Sci*, vol. 633, pp. 142–154, Mar. 2023, doi: 10.1016/j.jcis.2022.11.086.

[145] S. Huang, S. He, Y. Li, S. Wang, and X. Hou, "Hydrogen bond acceptor lined hydrogel electrolyte toward Dendrite-Free aqueous Zn ion batteries with low temperature adaptability," *Chemical Engineering Journal*, vol. 464, p. 142607, May 2023, doi: 10.1016/j.cej.2023.142607.

[146] Q. Li, L. Han, Q. Luo, X. Liu, and J. Yi, "Towards Understanding the Corrosion Behavior of Zinc-Metal Anode in Aqueous Systems: From Fundamentals to Strategies," *Batter Supercaps*, vol. 5, no. 4, Apr. 2022, doi: 10.1002/batt.202100417.

[147] Y. Shang and D. Kundu, "Understanding and Performance of the Zinc Anode Cycling in Aqueous Zinc-Ion Batteries and a Roadmap for the Future," *Batter Supercaps*, vol. 5, no. 5, May 2022, doi: 10.1002/batt.202100394.

[148] A. L. Zhu, D. P. Wilkinson, X. Zhang, Y. Xing, A. G. Rozhin, and S. A. Kulinich, "Zinc regeneration in rechargeable zinc-air fuel cells—A review," *J Energy Storage*, vol. 8, pp. 35–50, Nov. 2016, doi: 10.1016/j.est.2016.09.007.

[149] X. Guo and G. He, "Opportunities and challenges of zinc anodes in rechargeable aqueous batteries," *J Mater Chem A Mater*, vol. 11, no. 23, pp. 11987–12001, 2023, doi: 10.1039/D3TA01904G.

[150] S. Marquez-Bravo *et al.*, "Functional Bionanocomposite Fibers of Chitosan Filled with Cellulose Nanofibers Obtained by Gel Spinning," *Polymers (Basel)*, vol. 13, no. 10, p. 1563, May 2021, doi: 10.3390/polym13101563.

[151] B. Cao *et al.*, "Electrolyte Optimization Strategy: Enabling Stable and Eco-Friendly Zinc Adaptive Interfacial Layer in Zinc Ion Batteries," *Molecules*, vol. 29, no. 4, p. 874, Feb. 2024, doi: 10.3390/molecules29040874.

[152] H. Ge, X. Feng, D. Liu, and Y. Zhang, "Recent advances and perspectives for Zn-based batteries: Zn anode and electrolyte," *Nano Research Energy*, vol. 2, p. e9120039, Mar. 2023, doi: 10.26599/NRE.2023.9120039.

[153] Z. Zhao, X. Fan, J. Ding, W. Hu, C. Zhong, and J. Lu, "Challenges in Zinc Electrodes for Alkaline Zinc–Air Batteries: Obstacles to Commercialization," *ACS Energy Lett*, vol. 4, no. 9, pp. 2259–2270, Sep. 2019, doi: 10.1021/acsenergylett.9b01541.